

Effects of Strong Magnetic Fields on Neutron Star Structure

Christian Y. Cardall, Madappa Prakash, and James M. Lattimer

*Department of Physics & Astronomy, State University of New York at Stony Brook, Stony Brook,
NY 11794-3800*

November 6, 2000

ABSTRACT

We study static neutron stars with poloidal magnetic fields and a simple class of electric current distributions consistent with the requirement of stationarity. For this class of electric current distributions, we find that magnetic fields are too large for static configurations to exist when the magnetic force pushes a sufficient amount of mass off-center that the gravitational force points outward near the origin in the equatorial plane. (In our coordinates an outward gravitational force corresponds to $\partial \ln g_{tt} / \partial r > 0$, where t and r are respectively time and radial coordinates and g_{tt} is coefficient of dt^2 in the line element.) For the equations of state (EOSs) employed in previous work, we obtain configurations of higher mass than had been reported; we also present results with more recent EOSs. For all EOSs studied, we find that the maximum mass among these static configurations with magnetic fields is noticeably larger than the maximum mass attainable by uniform rotation, and that for fixed values of baryon number the maximum mass configurations are all characterized by an off-center density maximum.

Subject headings: stars: neutron — stars: magnetic fields

1. INTRODUCTION

Over the years, the typical magnitudes of the surface magnetic fields of pulsars—as inferred from measured spindown rates and simple magnetic dipole models—have been $\sim 10^{12} - 10^{13}$ G (Taylor, Manchester & Lyne 1993). Assuming magnetic flux conservation, fields of $\sim 10^{12}$ G would naturally arise from typical main sequence star surface magnetic fields of ~ 100 G during a decrease in radius by a factor of $\sim 10^5$ (Shapiro & Teukolsky 1983). At the extreme end of fields attainable by flux conservation, the largest observed white dwarf magnetic field of 5×10^8 G leads to a neutron star field of $\sim 1 \times 10^{14}$ G (Carroll & Ostlie 1996), while the largest observed main sequence stellar magnetic field of 3.4×10^4 G (Böhm-Vitense 1989) also suggests a possible field of a few times 10^{14} G.

Several independent circumstantial arguments link the class of objects known as “soft γ -ray repeaters” (SGRs), and perhaps the so-called “anomalous X-ray pulsars” (AXPs), with neutron stars having magnetic fields $\gtrsim 10^{14}$ G—the so-called “magnetars” (Duncan & Thompson 1992; Usov 1992; Paczyński 1992; Thompson & Duncan 1995, 1996; Vasisht & Gotthelf 1997). (Table 1 displays some observed properties of these objects.) In addition to the circumstantial arguments, more direct evidence for magnetic fields of $2 - 8 \times 10^{14}$ G is available for two of the five known SGRs, in the form of measured periods and spindown rates of associated X-ray pulsars (Kouveliotou et al. 1998, 1999).¹ Furthermore, the observed X-ray luminosities of the AXPs may require a field strength $B \gtrsim 10^{16}$ G (Chatterjee, Hernquist, & Narayan 2000; Heyl & Kulkarni 1998). The population statistics of SGRs suggest that magnetars may constitute a significant fraction ($\gtrsim 10\%$) of the neutron star population (Kouveliotou et al. 1994, 1998). As mentioned above, there are isolated examples of progenitor stars which could yield fields of $\sim 10^{14}$ G by flux conservation, but these isolated examples do not seem sufficient to account for a significant fraction of the neutron star population. Thus, it seems likely that some mechanism *generates* magnetic fields in nascent neutron stars. For example, Duncan & Thompson (1992) suggest that the smoothing out of differential rotation and convection could generate fields as large as $3 \times 10^{17} (P_i/1 \text{ ms})^{-1}$ G, where P_i is the initial rotation period of the neutron star.

These considerations motivate study of the effects of ultra-strong magnetic fields on neutron star properties. In this we have been inspired by the pioneering work of Bocquet, Bonazzola, Gourgoulhon & Novak (1995), who performed relativistic calculations of axisymmetric neutron star structure in which the standard stress-energy tensors of a perfect fluid and the electromagnetic field were employed, and were comparable in magnitude. The maximum fields they found were of order 10^{18} G, with increases of 13 to 29% in the maximum mass of nonrotating stars for various equations of state.

An additional motivation is provided by the recent findings that magnetic fields of strengths larger than 10^{16} G affect the EOS of dense matter directly through drastic changes in the composition of matter (Chakrabarty 1996; Chakrabarty, Bandyopadhyay, & Pal 1997; Yuan & Zhang 1999; Broderick, Prakash, & Lattimer 2000). The EOS is altered by both the Landau quantization of the charged particles (such as protons, electrons, etc.) and the interactions of the magnetic moments, including the anomalous magnetic moments of the neutral particles (such as the neutron, strangeness-bearing Λ -hyperon etc.) with the magnetic field. In this work, we consider only the effects of the magnetic field on the structure, through its influence on the metric, in order to facilitate a comparison with the earlier work of Bocquet et al. (1995). The additional changes caused by the direct effects of the magnetic field on the EOS will be reported in a future work (Cardall, Broderick, Prakash, & Lattimer 2000).

¹For ongoing discussion of this interpretation of X-ray timing data see e.g. Marsden et al. (1999a); Woods et al. (1999a); Harding et al. (1999); Marsden, Rothschild, & Lingenfelter (1999b); Chatterjee, Hernquist, & Narayan (2000).

While Bocquet et al. (1995) also presented solutions for rotating neutron stars endowed with large magnetic fields, in this work we present only static solutions. In terms of the potential observability of the effects of large magnetic fields, the most relevant situation appears to be for non-rotating stars. Neutron stars with the highest inferred magnetic fields—the so-called “magnetars”—are all observed to be rotating very slowly, with periods on the order of seconds. The effects of such slow rotation should have a negligible impact on the neutron star structure.

In this paper we extend the work of Bocquet et al. (1995). The theoretical formalism is outlined in §2, which serves to put the problem in context. In §3 we shed light on an issue left somewhat unclear by Bocquet et al. (1995): What physically determines the maximum mass and magnetic field for a given maximum density or given baryon mass? In order to explore these questions we have chosen to solve the structural equations using a Green’s function technique rather than the spectral technique employed by Bocquet et al. (1995), and we also searched for the maximum mass, for a given magnetic field distribution, in a different way. An appendix describes our numerical methods and tests of our code. In §4 we present an illuminating view of constant baryon mass and constant magnetic moment sequences, and present higher mass configurations than those found by Bocquet et al. (1995) for the equations of state (EOSs) they employed. In addition, we present the results of analogous calculations using three more recent EOSs. Summary and outlook are contained in §5.

2. FORMALISM

We consider stationary neutron star models in which the equation of state is independent of the magnetic field. The relevant equations and some properties of neutron stars in this limit were studied by Bonazzola et al. (1993) and Bocquet et al. (1995). The stress-energy tensor is given by the sum of the standard stress-energy tensors of a perfect fluid and the electromagnetic field:

$$T^{\alpha\beta} = (e + p) u^\alpha u^\beta + p g^{\alpha\beta} + \frac{1}{4\pi} \left(F^{\alpha\rho} F^\beta{}_\rho - \frac{1}{4} g^{\alpha\beta} F_{\rho\sigma} F^{\rho\sigma} \right), \quad (1)$$

where e and p are respectively the rest-frame energy density and pressure, u^α is the fluid 4-velocity, $g_{\alpha\beta}$ are the metric components, and $F_{\alpha\beta} \equiv A_{\beta,\alpha} - A_{\alpha,\beta}$, where A_α is the electromagnetic potential 1-form.

At least two relativistic formulations of the problem of strongly nonspherical axisymmetric stars have been developed. Most authors studying rapid rotation have adopted the approach of Bardeen & Wagoner (1971), which explicitly assumes an isotropic stress tensor and is thus incompatible with electromagnetic fields. Building on earlier work of Bonazzola & Maschio (1971) and Bonazzola & Schneider (1974), Bonazzola et al. (1993) present a formulation which allows for the most general stress-energy tensor consistent with a spacetime having the properties of stationarity, axisymmetry, and circularity. The metric for such a spacetime can be expressed as

$$g_{\alpha\beta} dx^\alpha dx^\beta = -e^{2\nu} dt^2 + e^{-2\nu} G^2 r^2 \sin^2 \theta (d\phi - N^\phi dt)^2 + e^{2(\zeta-\nu)} (dr^2 + r^2 d\theta^2), \quad (2)$$

where the metric functions ν , G , N^ϕ , and ζ are functions of (r, θ) . (A spacetime having the properties of stationarity and axisymmetry, but not circularity, would have an additional off-diagonal term in the metric (Bocquet et al. 1995; Carter 1973)). For the spacetime to have the property of circularity in addition to the properties of stationarity and axisymmetry, it is necessary that the electromagnetic current 4-vector and fluid 4-velocity be parallel to a general linear combination of the Killing vectors (Carter 1973). For example, in the coordinates of equation (2), J^t and J^ϕ would be the only nonvanishing components of the electromagnetic current 4-vector. A further consequence of this is that A_t and A_ϕ are the only nonvanishing components of the electromagnetic potential 1-form (Carter 1973).

From the Einstein equations, Bonazzola et al. (1993) derive a Poisson equation for each of the metric variables, with source terms that depend on the metric variables and on the components of the stress-energy tensor:

$$\Delta_3 \nu = \sigma_\nu, \quad (3)$$

$$\tilde{\Delta}_3 \tilde{N}^\phi = \sigma_{\tilde{N}^\phi}, \quad (4)$$

$$\Delta_2 \tilde{G} = \sigma_{\tilde{G}}, \quad (5)$$

$$\Delta_2 \zeta = \sigma_\zeta, \quad (6)$$

where

$$\tilde{N}^\phi \equiv r \sin \theta N^\phi, \quad (7)$$

$$\tilde{G} \equiv r \sin \theta G, \quad (8)$$

and Δ_2 , Δ_3 , and $\tilde{\Delta}_3$ are respectively the 2D flat space Laplacian, the 3D flat space Laplacian, and the ϕ component of the 3D flat space vector Laplacian:

$$\Delta_2 \equiv \frac{\partial^2}{\partial r^2} + \frac{1}{r} \frac{\partial}{\partial r} + \frac{1}{r^2} \frac{\partial^2}{\partial \theta^2}, \quad (9)$$

$$\Delta_3 \equiv \frac{\partial^2}{\partial r^2} + \frac{2}{r} \frac{\partial}{\partial r} + \frac{1}{r^2} \frac{\partial^2}{\partial \theta^2} + \frac{1}{r^2 \tan \theta} \frac{\partial}{\partial \theta}, \quad (10)$$

$$\tilde{\Delta}_3 \equiv \Delta_3 - \frac{1}{r^2 \sin^2 \theta}. \quad (11)$$

The source terms in equations (3-6) involve the metric functions and components of the stress-energy tensor:

$$\sigma_\nu = 4\pi G_N e^{2(\zeta-\nu)} (E + S^i_i) + \frac{1}{2} e^{-4\nu} G^2 r^2 \sin^2 \theta (\partial N^\phi)^2 - \partial \nu \partial (\ln G), \quad (12)$$

$$\sigma_{\tilde{N}^\phi} = -\frac{16\pi G_N e^{2\zeta+\nu}}{G^2} \frac{I_\phi}{r \sin \theta} - r \sin \theta \partial N^\phi \partial [\ln (e^{-4\nu} G^3)], \quad (13)$$

$$\sigma_{\tilde{G}} = 8\pi G_N e^{2(\zeta-\nu)} G r \sin \theta (S^r_r + S^\theta_\theta), \quad (14)$$

$$\sigma_\zeta = 8\pi G_N e^{2(\zeta-\nu)} S^\phi_\phi + \frac{3}{4} e^{-4\nu} G^2 r^2 \sin^2 \theta (\partial N^\phi)^2 - (\partial \nu)^2. \quad (15)$$

In these expressions the notation $\partial X \partial Y$ denotes

$$\partial X \partial Y \equiv \frac{\partial X}{\partial r} \frac{\partial Y}{\partial r} + \frac{1}{r^2} \frac{\partial X}{\partial \theta} \frac{\partial Y}{\partial \theta}. \quad (16)$$

In addition, G_N is Newton’s constant, and the contributions from the stress-energy tensor are²

$$E = T_{\alpha\beta} n^\alpha n^\beta, \quad (17)$$

$$I_\alpha = -h_{\alpha\beta} n_\rho T^{\beta\rho}, \quad (18)$$

$$S_{\alpha\beta} = h_{\alpha\rho} h_{\beta\sigma} T^{\rho\sigma}, \quad (19)$$

where n^α is the unit four vector orthogonal to the spacelike time slices and $h_{\alpha\beta} = g_{\alpha\beta} + n_\alpha n_\beta$ is the spacelike projection tensor. In the present coordinates $n_\alpha = (-N, 0, 0, 0)$, where $N = e^\nu$ is the lapse function. For the stress-energy tensor of a perfect fluid [the first part of equation (1)],

$$E^{\text{PF}} = \Gamma^2(e + p) - p, \quad (20)$$

$$(I^{\text{PF}})_\phi = e^{-\nu} G r \sin \theta (E^{\text{PF}} + p) U, \quad (21)$$

$$(S^{\text{PF}})^r_r = p, \quad (S^{\text{PF}})^\theta_\theta = p, \quad (S^{\text{PF}})^\phi_\phi = p + (E^{\text{PF}} + p) U^2, \quad (22)$$

where $\Gamma = (1 - U^2)^{-1/2}$ and $U = e^{-2\nu} G r \sin \theta (\Omega - N^\phi)$, and the superscript “PF” stands for “perfect fluid.” In this expression for U , the scalar Ω is the angular velocity as measured by a static observer at infinity; it relates the nonvanishing components of u^α through the equation $u^\phi = \Omega u^t$.³ For the standard stress-energy tensor of the electromagnetic field [the last two terms of equation (1)], restricted to a poloidal field, we have

$$E^{\text{EM}} = \frac{1}{8\pi} (E_i E^i + B_i B^i), \quad (23)$$

$$(I^{\text{EM}})_\phi = \frac{1}{4\pi} e^{2\zeta - 3\nu} G r^2 \sin \theta (E^r B^\theta - E^\theta B^r), \quad (24)$$

$$(S^{\text{EM}})^r_r = \frac{1}{8\pi} (E_\theta E^\theta - E_r E^r + B_\theta B^\theta - B_r B^r), \quad (25)$$

$$(S^{\text{EM}})^\theta_\theta = -(S^{\text{EM}})^r_r, \quad (S^{\text{EM}})^\phi_\phi = E^{\text{EM}}, \quad (26)$$

in which the superscript “EM” identifies the electromagnetic contributions. In these expressions E_i and B_i are the components of the electric and magnetic fields as measured by an Eulerian observer (i.e. an observer with four velocity n^α):

$$E_\alpha = n^\beta F_{\alpha\beta} \quad (27)$$

²We do not use E to denote the magnitude of the electric field, although we will use the subscripted notation E_i to refer to components of the electric field.

³As will be discussed below, in the limit of infinite conductivity (“frozen-in magnetic fields”), stationary stars with magnetic fields must be uniformly rotating.

$$= \left(0, e^{-\nu} \left[\frac{\partial A_t}{\partial r} + N^\phi \frac{\partial A_\phi}{\partial r} \right], e^{-\nu} \left[\frac{\partial A_t}{\partial \theta} + N^\phi \frac{\partial A_\phi}{\partial \theta} \right], 0 \right), \quad (28)$$

$$B_\alpha = -\frac{1}{2} \epsilon_{\alpha\beta\rho\sigma} n^\beta F^{\rho\sigma} \quad (29)$$

$$= \left(0, \frac{e^\nu}{Gr^2 \sin \theta} \frac{\partial A_\phi}{\partial \theta}, -\frac{e^\nu}{G \sin \theta} \frac{\partial A_\phi}{\partial r}, 0 \right), \quad (30)$$

where $\epsilon_{\alpha\beta\rho\sigma}$ is the Levi-Civita tensor.

The quantities A_t and A_ϕ are also determined by Poisson equations, which derive from the Maxwell equations in curved spacetime (Bocquet et al. 1995):

$$\Delta_3 A_t = \sigma_{A_t}, \quad (31)$$

$$\tilde{\Delta}_3 \tilde{A}^\phi = \sigma_{\tilde{A}^\phi}, \quad (32)$$

where $\tilde{A}^\phi \equiv A_\phi / (r \sin \theta)$. The sources can be expressed

$$\begin{aligned} \sigma_{A_t} &= -4\pi e^{2(\zeta-\nu)} \left(g_{tt} J^t + g_{t\phi} J^\phi \right) + e^{-2\nu} g_{t\phi} \partial A_t \partial N^\phi - (2 + e^{-2\nu} g_{tt}) \partial A_\phi \partial N^\phi \\ &\quad - (\partial A_t + 2N^\phi \partial A_\phi) \partial \left[\ln(e^{-2\nu} G) \right] - \frac{2N^\phi}{r} \left(\frac{\partial A_\phi}{\partial r} + \frac{1}{r \tan \theta} \frac{\partial A_\phi}{\partial \theta} \right), \end{aligned} \quad (33)$$

$$\begin{aligned} \sigma_{\tilde{A}^\phi} &= -4\pi e^{2\zeta-4\nu} G^2 r \sin \theta \left(J^\phi - N^\phi J^t \right) + e^{-4\nu} G^2 r \sin \theta \partial N^\phi \left(\partial A_t + N^\phi \partial A_\phi \right) \\ &\quad + \frac{1}{r \sin \theta} \partial A_\phi \partial \left[\ln(e^{-2\nu} G) \right]. \end{aligned} \quad (34)$$

A theorem of Cowling (1934) states that an axisymmetric magnetic field cannot be generated or maintained by the motion of a fluid. The theorem relies on the fact that finite resistivity involves dissipation, leading to magnetic field decay.⁴ Hence stationary models of neutron stars in magnetic fields require a separation of dynamical and dissipative time scales, encoded in an assumption of infinite conductivity [magnetic fields “frozen in” and carried with the fluid, a common assumption in astrophysics (Alvén 1950)]. This assumption is exceedingly well justified for neutron star matter, the Ohmic dissipation time scale being larger than the age of the universe (Goldreich & Reisenegger 1992). Cowling’s theorem is thus effectively nullified. In addition, as shown by Bonazzola et al. (1993), the assumption of infinite conductivity leads to the requirement of uniform rotation, as well as the relation

$$A_t = -\Omega A_\phi + \text{const} \quad (35)$$

inside the star, where the constant is determined by the total electric charge of the star.

Closure of the system of equations requires relations involving some quantities appearing in the source equations (12-15) and (33-34): the rest-frame energy density e and pressure p , and

⁴Ambipolar diffusion and Hall drift (Goldreich & Reisenegger 1992) will actually dominate magnetic field decay in magnetars, but even for the ultra strong fields considered here the decay time will be hundreds if not thousands of years.

the components J^t and J^ϕ of the electromagnetic 4-current. For a uniformly rotating stationary star in a magnetic field, local energy-momentum conservation ($T^{\alpha\beta}_{;\beta} = 0$) yields the equations of stationary equilibrium: (Bonazzola et al. 1993)

$$\frac{1}{e+p} p_{,i} + \nu_{,i} - (\ln \Gamma)_{,i} - \frac{1}{e+p} F_{i\alpha} J^\alpha = 0, \quad (36)$$

in which $X_{,i} \equiv \partial X / \partial x^i$. Derivatives with respect to the coordinates $x^i = (r, \theta)$ give the only nontrivial equations, due to the symmetries of the problem. We recall that $\nu \equiv (1/2) \ln(-g_{tt})$ here plays a role like that of the gravitational potential in the Newtonian case, and that Γ is the Lorentz factor associated with the fluid’s rotational velocity. By analogy with the Newtonian case, the terms in equation (36) may be thought of as (from left to right) the pressure force, gravitational force, centrifugal force, and Lorentz force.

For a one-parameter equation of state, $e = e(n)$, $p = p(n)$, there is a first integral of the first term in equation (36):

$$h(n) = \int_0^n \frac{1}{e(n') + p(n')} \frac{dp}{dn'} dn', \quad (37)$$

where we will assume that $h(0) = 0$ corresponds to the surface of the star.⁵ This, together with the adoption of a “current function” $f(A_\phi)$,

$$\frac{1}{e+p} (J^\phi - \Omega J^t) = f(A_\phi), \quad (38)$$

give the equations of hydrostatic equilibrium a first integral (Bonazzola et al. 1993):

$$h(r, \theta) + \nu(r, \theta) - \ln \Gamma(r, \theta) + M(r, \theta) = C = \text{constant}, \quad (39)$$

where the “magnetic potential” $M(r, \theta)$ is given by

$$M(r, \theta) = M(A_\phi(r, \theta)) = - \int_0^{A_\phi(r, \theta)} f(x) dx. \quad (40)$$

While one is free to choose the current function $f(A_\phi)$, equation (38) represents a significant restriction on the form of the electromagnetic current that allows the existence of stationary solutions. The constant C is determined by an input parameter, e.g. the density specified at some point in the star.

In summary, the formalism of stationary neutron stars in poloidal magnetic fields with a one-parameter equation of state consists of a closed system of eleven variables [four metric variables, energy density, pressure, two components of the electromagnetic potential, two components of the

⁵For example, at zero temperature and in chemical equilibrium, the pressure and energy density are functions only of the baryon density n . By virtue of the first law of thermodynamics, $h(n)$ is seen to be the logarithm of the enthalpy per baryon: $h = \ln[(e+p)/n] + \text{constant}$.

electromagnetic current, and the “heat function” h of equation (37)]; eleven equations [four Poisson equations (3–6) for the metric variables, two Poisson equations (31–32) for the components of the electromagnetic potential, the relation (35) between the components of the electromagnetic potential, the equation of state, the relation (37) between the heat function and e and p , the first integral (39) of the equations of hydrostatic equilibrium, and the restriction (38) on the electromagnetic current]; three input parameters (angular velocity, total electric charge, and maximum density); and one input function [the $f(A_\phi)$ in equation (38)].

3. WHEN IS THE MAGNETIC FIELD TOO LARGE?

As noted in the introduction, in this study we restrict ourselves to the static case. This involves a number of simplifications, including the vanishing of N^ϕ , A_t and J^t , and the absence of surface charges generally present on perfectly conducting rotating bodies.

Bocquet et al. (1995) present numerical calculations aimed at determining “the maximum mass configuration among all static magnetized models” for several equations of state and for the choice of constant current function $f(A_\phi) = f_0$. These static configurations are determined by two parameters, which Bocquet et al. (1995) took to be the central density and f_0 . They considered sequences of constant magnetic dipole moment \mathcal{M} , which is defined in terms of the asymptotic behavior of (the orthonormal components of) the magnetic field,

$$(2\mathcal{M} \cos \theta / r^3) = B_{(r)}|_{r \rightarrow \infty} = (e^{2\nu - \zeta} / Gr^2 \sin \theta) (\partial A_\phi / \partial \theta)|_{r \rightarrow \infty}, \quad (41)$$

and then determined the maximum mass for each value of \mathcal{M} . For example, using the “Pol2” $\gamma = 2$ polytropic equation of state (Salgado et al. 1994), they reported the maximum mass among all static configurations to be $4.062M_\odot$, with a magnetic moment of 1.122×10^{33} A m². We have calculated, also using the Pol2 EOS, a similar configuration, which is pictured in Figure 1, and may be compared with Figures 5 and 6 of Bocquet et al. (1995). We point out that in Figures 1 through 6 that we use the same polytropic constant in the Pol2 EOS as that employed by Bocquet et al. (1995). However, in later figures and in all tables, we have altered the polytropic constant to a more realistic value so that the maximum mass of static configurations is $2.0M_\odot$, and then scaled the results from the other groups accordingly in these tables and figures.

Bocquet et al. (1995) also note that “For magnetic fields higher than [this configuration], no stationary configuration can exist and the numerical procedure... fails to converge.” Note that this is not a question of *stability*—nothing is being claimed about the stability of the high field configurations they achieve—the question pertains to even the *existence* of stationary solutions. The fact that the maximum mass and magnetic moment are determined by the failure of their code to converge leaves one wondering whether a genuine physical limit has been reached, or whether the result simply represents the failure of the numerical method to find solutions that do in fact exist.

This situation is in contrast to the case of rotation: It is well known that there is an upper limit to the angular velocity of uniformly rotating stars. Numerical codes that attempt to solve for stellar configurations with uniform angular velocities above this limit will fail to converge. However, there is also a well-defined physical basis for this “Keplerian” limit, namely, mass shedding.⁶

At the mass shedding limit, a fluid element at the equatorial surface undergoes geodesic motion: it can remain in that orbit without any pressure support from the star. Thus, it is not necessary to rely only on the failure of the code to converge to determine the mass shedding limit; one can quantitatively test for geodesic motion at the equatorial surface.

The approach to the mass shedding limit can also be visualized using the first integral of the equations of hydrostatic equilibrium—the relativistic generalization of the Bernoulli equation. From equation (39), the “Bernoulli equation” for a uniformly rotating star without a magnetic field is

$$h(r, \theta) + \nu(r, \theta) - \ln \Gamma(r, \theta) = C = \text{constant}. \quad (42)$$

Figure 2 demonstrates how the Bernoulli equation can be used to visualize the approach to the mass shedding limit. In this figure the dashed lines represent ν , the dot-dashed lines represent $-\ln \Gamma$, and the thick solid lines represent $\nu - \ln \Gamma$, all as functions of a compactified radial coordinate in the equatorial plane. The dotted lines represent C , so that h is given by the distance between the dotted and thick solid lines. The surface of the star ($h = 0$) then corresponds to the intersection of the dotted and thick solid lines. In the lower panel of Figure 2, which represents the mass shedding limit, the equatorial surface of the star coincides with the maximum of $\nu - \ln \Gamma$. For larger angular velocities, C would be larger than this maximum, and there would be no surface of the star at finite radius.

Similar plots can be made for stationary stars with magnetic fields. For a nonrotating star in a poloidal magnetic field, equation (39) reduces to

$$h(r, \theta) + \nu(r, \theta) + M(r, \theta) = C = \text{constant}. \quad (43)$$

Now, in the equatorial plane, along which direction are magnetic forces exerted? The answer depends on the direction of the magnetic field, which in turn depends on the current distribution in the star. From equation (38) (with Ω and J^t set to zero in the present static case), the electric current density is proportional to $(e + p)$, so that in the typical case one would expect the current to vanish on the surface of the star. The current measured by a local observer must also vanish on the axis of symmetry. Hence the current $J^{(\phi)}$ measured by a local observer in the equatorial plane is expected to have a structure that peaks somewhere inside the star and vanishes at the origin and

⁶In reality, the rotation may be more severely limited by a gravitational instability to non-axisymmetric perturbations. The instability might, however, be damped out by bulk and shear viscous effects (Lindblom, & Detweiler (1977); Imamura, Durisen, & Friedman (1985); Friedman, Ipser, & Parker (1986); Ipser, & Lindblom (1989); Sawyer (1989)) To the extent that the Keplerian limit represents a reasonable estimate of the upper limit of rotation, our analysis here illuminates the stark contrasts that exist between the instabilities caused by rotation and magnetic fields.

the surface, as shown in the left panel of Figure 3 for the Pol2 EOS. Since the magnetic field lines tend to circle around a point in the vicinity of the maximum current (see the right panel in Figure 1), in the equatorial plane the field reverses direction inside the star. Accordingly, the Lorentz force reverses direction inside the star, as displayed in the right panel of Figure 3.

The Lorentz force and the other “forces” acting in the equatorial plane are derivatives of the quantities appearing in equation (43). These quantities are plotted in Figure 4 for the Pol2 EOS, which is similar to Figure 2, except that the dot-dashed lines now represent the magnetic potential $M(r, \theta)$ in equation (39), given in this case by equation (40) with $f = \text{constant} = f_0$. In the inner portion of the star, the Lorentz force behaves like a centrifugal force, pushing outward and allowing the star to support more mass. As seen in the lower panel of Figure 4 (and in the left panel of Figure 1), this outward force can be strong enough to cause the maximum of h (and hence e) to be off-center. However, the reversal of the force at larger radii makes the total “potential” confining. Thus, in contrast to the case of rotation, there is no mass shedding limit at the equatorial surface that clearly indicates the nonexistence of stationary solutions and explains the failure of the code to converge for large magnetic fields.

If mass shedding does not occur, is there some other identifiable physical cause that prevents the existence of stationary solutions for sufficiently large magnetic fields? Bocquet et al. (1995) note that for sufficiently large fields, the total (fluid + magnetic) stress tensor has a component on the symmetry axis that goes from being positive (pressure) to negative (tension), causing the star to have a characteristic “pinched” shape (see the left panel of Figure 1). This occurs when the “magnetic pressure” exceeds the fluid pressure. They note that in the largest mass configurations they obtain, the ratio of the magnetic to fluid pressures at the center of the star is of order unity. However, there are two reasons that argue against considering this as a definitive physical reason preventing the existence of stationary solutions. The first is a matter of principle: the equilibrium of fluid elements relies on a balance between gravity and the *gradients* of stresses; the absolute sign of the stresses themselves is not of fundamental importance. The second reason is the results observed in practice: the value of the ratio of magnetic pressure to fluid pressure at the center of the star reported by Bocquet et al. (1995), for the putative maximum mass configurations, varies quite noticeably among different equations of state, and its value is not predictable. This is not what one would expect of a precise physical criterion for the nonexistence of stationary solutions.

For Newtonian stars, Chandrasekhar & Fermi (1953) identified gravitational binding, or a negative total energy (excluding rest mass), as a necessary criterion for the dynamical stability of equilibrium solutions. For nonrotating polytropes, they used a generalization of the virial theorem that accounts for magnetic fields to show that a negative total energy requires that the magnitude of the gravitational potential energy must be greater than the magnetic field energy.

One might wonder whether a criterion of gravitational binding could represent a physical upper limit on stellar magnetic fields in the relativistic case as well. While total gravitational and magnetic energies are not well defined in relativity, in some sense the gravitational mass M

contains all forms of “energy,” including “magnetic energy.” Since the total baryon number [or total baryon mass $M_B = (\text{baryon mass}) \times (\text{baryon number})$] is a well defined quantity, one might consider using the relation $M - M_B < 0$ as a criterion for gravitational binding. As it turns out, the putative maximum mass and maximum field configurations reported by Bocquet et al. (1995) are still “gravitationally bound” by this criterion. The question remains: As the influence of the magnetic field increases, is this apparent transition from existence to nonexistence of static solutions, occurring at finite “gravitational binding,” a physical result or a numerical artifact?

In order to explore these questions we have searched for the maximum mass in a different way than Bocquet et al. (1995). As mentioned previously, Bocquet et al. (1995) computed sequences of constant magnetic moment \mathcal{M} by suitably adjusting the central log-enthalpy h_c and the value f_0 of the (constant) current function f . For each value of \mathcal{M} they determined the maximum mass. The overall maximum mass was obtained with the largest value of \mathcal{M} for which convergence could be achieved. In contrast, we have chosen a more direct means of exploring parameter space. For each value of maximum log-enthalpy h_{max} (which for large fields will *not* coincide with h_c), we found the largest values of f_0 for which the code converged. Specifying h_{max} instead of h_c allows for the possibility of vanishing density at the origin, i.e. toroidal configurations.

A close inspection of the forces in configurations near the failure to converge reveals an apparent physical cause, for the choice of constant current function, of the failure to find stationary solutions for sufficiently large magnetic fields: *When a sufficient quantity of matter has been pushed off-center by magnetic forces that gravitational forces begin to point radially outward in the equatorial plane, a topological change to a toroidal configuration ensues.* This is illustrated by Figure 5 for the Pol2 EOS, which shows the late stages of iteration of a configuration with a value of f_0 that is slightly too large for convergence. We emphasize that the stages depicted in this figure are not valid stationary solutions to the Einstein equations; neither do they represent a true evolution. Nevertheless, the sequence is suggestive of possible dynamical outcomes: a transition to a toroidal topology, expansion of the torus to large radii, and increasing compactification of the toroidal configuration of matter. As the iterations proceed, the outward pointing gravitational force (positive $-\partial\nu/\partial s$ or $-\partial\nu/\partial r$) becomes more and more pronounced. The central evacuation begins, however, with a tiny outward gravitational force at some radius.

Since we were unable to find any convergent toroidal solutions for the case of a constant current function f , we can therefore identify a quantitative criterion for the boundary of existence of stationary solutions in this case: this boundary is characterized by $\partial\nu/\partial r = 0$ at some off-center location in the equatorial plane. By symmetry, it is always the case that $\partial\nu/\partial r = 0$ at the origin; furthermore, the positive-semidefiniteness of energy density and pressure ensure that $\partial^2\nu/\partial r^2 \geq 0$ at the origin (this can be verified from the Green’s function expansions of the metric functions presented in Appendix A). This means that the critical condition $\partial\nu/\partial r < 0$ cannot occur at the origin or an infinitesimal region surrounding it, but our numerical calculations indicate that it first occurs very close to the origin.

These matters are illustrated in Figure 6 with the Pol2 EOS, which shows the radial profile of the gravitational force for increasing values of f_0 —at a particular value of maximum density— including the largest value of f_0 for which convergence was achieved. In the upper panel, a flattening of the gravitational force near the center with increasing magnetic field is apparent. The insets in the upper panel show the region near the origin. The lower left inset shows $-\partial\nu/\partial r$ as computed with a formula obtained by differentiating equation (A2). As required by the condition $\partial^2\nu/\partial r^2 \geq 0$ at the origin, according to this formula the first off-origin grid point has negative value of $-\partial\nu/\partial r$. For the largest value of f_0 , the next grid point is less negative, but still does not reach our asserted condition $-\partial\nu/\partial r = 0$. However, the upper right inset in the upper panel shows values of $-\partial\nu/\partial r$ near the origin computed from a centered finite difference formula, which is closer to what the discretized configuration actually “feels.” Computed in this way, the first off-origin grid point has a barely positive value of $-\partial\nu/\partial r$ for the largest value of f_0 for which convergence was achieved. The lower panel of Figure 6 shows the gravitational force for the largest value of f_0 , for three different grid resolutions. The insets of this panel again compare the “analytic” and “numerical” derivatives. These computations show that with increasing resolution, the “analytic” derivative near the origin gets closer and closer to the critical condition $-\partial\nu/\partial r = 0$. In practice, however, the maximum mass and magnetic field configuration for a given stellar maximum density can be identified by the appearance of a small positive value of $-\partial\nu/\partial r$, as computed with a centered finite difference.

For the values of maximum density we studied, and for a constant current function f , we did not find any stationary toroidal solutions. The toroidal configurations continued to expand in radius and compress into thinner and thinner rings until the region covered by matter consisted of only a few gridpoints, at which point the code would fail. A determination of the outcome of the evolution of such configurations—whether to a stationary solution characterized by a different current function, dispersal to infinity, or even the formation of a toroidal event horizon (Shapiro, Teukolsky, & Winicour 1995)—would appear to require a fully relativistic evolution code.

It remains to be seen if these results—namely, the prescription for determining when magnetic forces are too strong for the existence of static configurations, and the lack of converged toroidal solutions—will hold for more general current functions.

4. SEQUENCES OF CONSTANT BARYON MASS AND CONSTANT MAGNETIC MOMENT

Our computations of static neutron stars with ultra-strong magnetic fields determined by a constant current function are summarized in Table 2 and Figures 7 and 8. Figure 7 contains some of the older EOSs employed by Bocquet et al. (1995). These include BJI, which is model IH of Bethe & Johnson (1974) [we derived our table from that listed in Malone, Johnson, & Bethe (1975)], and PandN, which is from Pandharipande (1971). Results for more recent EOSs are displayed in Figure 8. These include Akmal, which is from Akmal et al. (1998) and is based on a potential model description of dense matter and represents the most complete study to date in

which many-body and special relativistic corrections are incorporated. PCL is taken from Prakash et al. (1995), and is based on a relativistic field-theoretical description of dense matter starting from the Lagrangian proposed by Zimanyi & Moszkowski (1990). This approach easily allows for the inclusion of additional softening components: the case in which hyperons are present is labelled PCLhyp. For all EOSs except Pol2, we employed the EOS of Baym, Bethe, & Pethick (1971) and Baym, Pethick, & Sutherland (1971) at densities below about 1/2 the nuclear saturation density.

The rationale for exploring a wide variety of EOSs, even some that are relatively outdated, is two-fold. First, it provides contrasts among widely different theoretical paradigms. Second, it illuminates general relationships that exist between the pressure-density relation and the macroscopic properties of the star such as the maximum mass and the radius.

In these figures the lower thick solid curves show the gravitational mass M as a function of radius for static stars without magnetic fields, which are spherical. The upper thick solid curves show the outer boundaries beyond which no static solutions were found (see §3). The lighter solid curves are sequences of constant baryon mass M_B (and varying magnetic moment \mathcal{M}), while the dotted curves are sequences of constant magnetic moment (and varying baryon mass). The lighter shaded regions indicate configurations in which the magnetic field is sufficiently strong that the maximum density is off-center. The small slivers of darkly shaded regions towards the left sides of the plots indicate solutions which are gravitationally unbound ($M - M_B > 0$); these are expected to be dynamically unstable.

As with rotation, magnetic fields allow neutron stars with a particular EOS and baryon number to have larger masses and equatorial radii compared to the field-free case. In Figures 7 and 8, the configurations of maximum mass that can be reached by uniform rotation (without magnetic fields) are marked with an “X”. For all the EOSs displayed, our result for the maximum mass attainable with a magnetic field governed by a constant current function is noticeably larger than that attained by rotation. This contrasts with the results reported by Bocquet et al. (1995) for the maximum mass attainable with magnetic fields, shown in Figure 7 with crosses. Out of the three EOSs we have in common, only in the case of the polytropic EOS do Bocquet et al. (1995) obtain a significantly larger mass with magnetic fields than with rotation.

In the absence of significant accretion, constant baryon mass sequences are of interest as potential evolutionary paths. This is well motivated in the case of uniformly rotating non-magnetic stars: As angular momentum is slowly dissipated by gravitational radiation, the star moves along a sequence of constant baryon mass until it either stops rotating (for “normal” sequences terminating on the spherical mass vs. radius curve) or collapses to a black hole [for “supramassive” sequences which exist solely by virtue of rotation; stars on such sequences may exhibit the interesting phenomenon of spin-up during angular momentum loss just before collapse to black hole (Cook, Shapiro, & Teukolsky 1992, 1994a,b; Salgado et al. 1994)]. These scenarios are well motivated because of the expectation that once viscosity brings a dynamically stable star into uniform rotation, it will not spontaneously begin to differentially rotate as it loses angular momentum.

On the other hand, representing evolutionary sequences by the constant baryon mass sequences for magnetized stars pictured in Figures 7 and 8 is an oversimplification. Even though a star’s magnetic field will slowly (on dynamical time scales) decay due to Hall drift and ambipolar diffusion, there is no guarantee that the star’s configuration will proceed along the paths pictured in the figures. This is because the case of magnetic fields is more analogous to differential rotation rather than uniform rotation, the necessary choice of a current function in the magnetic case [see equation (38) and surrounding discussion] corresponding to the choice of a rotation law in the case of differential rotation. As a star’s magnetic field decays, it is not obvious that its current function will remain the same.⁷ Perhaps the study of several different current functions could shed light on probable evolutionary sequences. For example, an analysis of how the mass varies with the functional form of the current function (at fixed baryon mass and magnetic moment) could give an idea of how the slow evolution with magnetic field decay might proceed. There is of course no principle of “conservation of magnetic moment,” but since the time scale for magnetic field decay is slow, this procedure seems like a plausible opening exploration.

In connection with the constant baryon mass sequences, we here comment on a curious feature in Figures 7 and 8. For the potential model EOSs BJI, PandN and Akmal, the topology of these sequences near the maximum spherically symmetric star appears to be different than for the polytropic or relativistic field theoretical models PCL and PCLhyp. In the former, there is a minimum in the baryon mass above the spherical, non-magnetized, sequence. To determine if this feature was related to the possible acausal behavior of potential models at high density, we modified the PandN EOS to go over to a causality limit EOS when necessary, but found that the topology was unaltered. Instead, the effect appears to be related to the fact that all forms of energy contribute to the magnetic field: While the Newtonian intuition (and the relativistic behavior at lower densities) is that magnetic fields always increase the gravitational mass of a star of given baryon number, the fact that the energy density in magnetic fields can be a nontrivial source of gravitation means that this self-gravitating tendency can compete with the tendency of the Lorenz force to help support the star. Perhaps this occurs near the spherical maximum mass in the case of the potential model EOSs, with the result that configurations near the spherical maximum mass have nowhere to go but down in gravitational mass when magnetic fields (governed by a constant current function) are added. If a star did preserve its current function and follow a supramassive constant baryon mass sequence possessing such a gap, upon reaching the minimum mass of the sequence it could catastrophically collapse to a spherical neutron star rather than a black hole. While the possibility is admittedly remote, this could be a novel form of energy release in a baryon-free environment, giving rise to a mini- γ -ray burst.

Except for the spherical stars, those with no magnetization indicated by the lower solid line in these figures, the stability of the configurations has not been studied. For spherical stars, it

⁷Note that constant current function is *not* analogous to uniform rotation. Formally, the analogue to uniform rotation would be uniform magnetic vector potential, which of course means no magnetic field.

is well-known that the configurations with larger radii than the maximum mass configuration are stable. One might speculate that constant baryon mass sequences which terminate on the stable side of the spherical M vs. R curve are stable, while those ending on the unstable side would be unstable, and that for supramassive constant baryon mass sequences the minimum mass marks a change from stability to instability. But this remains to be determined. As with differentially rotating stars, it is necessary to do a normal mode analysis, or even a fully relativistic evolution; see Baumgarte, Shapiro, & Shibata (2000). Incidentally, it is interesting to note that these authors find a differentially rotating configuration with a “red blood cell” shape similar to our extreme magnetic configurations, and that this configuration is dynamically stable. Of course, their configuration was not subject to MHD instabilities that may come into play (Spruit 1999a,b).

5. SUMMARY AND OUTLOOK

In summary, we present a method of computing the structure of axisymmetric relativistic stars that combines elements of previous approaches, and report tests of our code. A quantitative method of determining the outer envelope (in the mass vs. radius plane) of configurations attainable with poloidal magnetic fields governed by a constant “current function” [see equation (38)] has been found: magnetic fields are too large for static configurations to exist when the magnetic force pushes a sufficient amount of mass off-center that the gravitational force points outward near the origin in the equatorial plane. (In our coordinates an outward gravitational force corresponds to $-\partial\nu/\partial r > 0$.) We obtain larger masses of neutron stars in ultra-strong magnetic fields than have been reported previously for various equations of state, and performed computations with three representative modern EOSs. Sequences of constant baryon mass and constant magnetic moment are displayed. For all EOSs studied, the maximum attainable mass of static stars with a magnetic field determined by a constant current function is noticeably larger than that attainable with uniform rotation and no magnetic field.

The results presented here are only an initial step in exploring possible configurations of neutron stars with strong magnetic fields. As we mention below, configurations with azimuthal field components will be of physical interest, which implies that three-dimensional geometries should also be considered. But even with attention restricted to poloidal fields, we have only scratched the surface of possible configurations, as we have only considered a single current function. Bocquet et al. (1995) make brief mention of computations with a few other current functions. We have performed a handful of exploratory computations using a polytropic EOS and other current functions and have found some toroidal solutions. These toroidal solutions were not attainable with the computational approach of Bocquet et al. (1995), since their method involved the specification of a finite density at the center of the star. In the case of toroidal configurations, the simple condition determining the boundary of existence of static configurations will have to be generalized, since there is no matter at the center. These explorations will be reported in detail elsewhere.

Our work here has focused on the effects magnetic fields have on general relativistic structure,

ignoring the effects of intense magnetic fields on the EOSs. Recently, the direct effects of magnetic fields on the EOS have also been investigated (Chakrabarty 1996; Chakrabarty, Bandyopadhyay, & Pal 1997; Yuan & Zhang 1999; Broderick, Prakash, & Lattimer 2000). Substantial effects on the EOS above nuclear saturation densities are generally produced by fields in excess of 10^{18} G, which is of the order of the maximum central field strengths found in this paper. The generic effects on the EOS include softening due to Landau quantization, which is, however, overwhelmed by stiffening due to the incorporation of the magnetic moments of the various particles in neutron star matter (Broderick, Prakash, & Lattimer 2000). (Note that the important $B^2/8\pi$ term is already included in our study.) Work is in progress (Cardall et al. 2000, in preparation) to provide fully self-consistent calculations of neutron star structure, in which the direct effects of magnetic fields on the EOS will be included in addition to the structural effects considered in this work.

An issue which we defer to future work is the question of stability. For systems governed by a finite number of parameters, a generalization (Sorkin 1982) of the familiar one-dimensional turning point method can be employed; see Friedman, Ipser, & Sorkin (1988) for an application to uniformly rotating relativistic stars. However, as with differentially rotating stars, this generalized turning point method is not really applicable in the present case. This is because the need to specify a current function (or rotation law in the case of differential rotation) means that defining a particular configuration requires the specification of an *infinite* number of parameters.

Another issue that needs further explication before the physical relevance of the results presented here can be fully assessed is the generation of magnetic fields. We have mentioned the mechanism of Duncan & Thompson (1992), the generation of magnetic fields during the smoothing of differential rotation. However, the azimuthal dragging of field lines by differential rotation leads to nonvanishing azimuthal field components, in contrast to the poloidal fields studied here. It is not clear whether fields with azimuthal components would evolve into poloidal configurations, or whether there are mechanisms to directly generate strong poloidal fields. It would be of interest to explore the possibility of finding stationary solutions with toroidal magnetic fields, and in three dimensions. While this would involve more nonzero metric components, perhaps methods similar to those employed in this paper could be employed; see Bonazzola, Gourgoulhon, & Marck (1998).

We wish to thank E. Gourgoulhon for helpful communications concerning the calculations of Bocquet et al. (1995). We are grateful to Dany Page and Ralph Wijers for their help in the preparation of Table 1. Research support from DOE grants FG02-87ER40317 (for CYC and JML) and FG02-88ER-40388 (for MP) are gratefully acknowledged.

A. NUMERICAL PROCEDURES AND TESTS OF THE CODE

Bonazzola et al. (1993) have developed a “spectral method” to solve equations (3-6). This method involves expanding the solution on a set of basis functions having the analytical properties of the solution. They also try to choose basis functions for which there exist fast transform algorithms.

Their method involves the use of two grids, an “inner” region including the origin and an “outer” region that reaches to infinity. Instead of this “spectral method,” we have chosen to solve the Poisson equations using Green’s functions, similar to the methods of Komatsu, Eriguchi, & Hachisu (1989) and Cook, Shapiro, & Teukolsky (1992, 1994a,b). It is convenient to compactify the radial domain $0 \leq r \leq \infty$ to $0 \leq s \leq 1$ via the change of variables

$$r = R \left(\frac{s}{1-s} \right), \tag{A1}$$

where R is some length scale. Taking into account the azimuthal and equatorial symmetries, and imposing the boundary conditions [all metric functions finite at the origin; $(\nu, N^\phi, \zeta)|_{r \rightarrow \infty} \rightarrow 0$, $G|_{r \rightarrow \infty} \rightarrow 1$], we find equations (3-6) to yield

$$\begin{aligned} \nu(s, \theta) = & - \sum_{n=0}^{\infty} P_{2n}(\cos \theta) \times \\ & \left[\left(\frac{1-s}{s} \right)^{2n+1} \int_0^s \frac{ds' s'^{2n}}{(1-s')^{2n+2}} \int_0^{\pi/2} d\theta' \sin \theta' P_{2n}(\cos \theta') \tilde{\sigma}_\nu(s', \theta') \right. \\ & \left. + \left(\frac{s}{1-s} \right)^{2n} \int_s^1 \frac{ds' (1-s')^{2n-1}}{s'^{2n+1}} \int_0^{\pi/2} d\theta' \sin \theta' P_{2n}(\cos \theta') \tilde{\sigma}_\nu(s', \theta') \right], \end{aligned} \quad (\text{A2})$$

$$\begin{aligned} N^\phi(s, \theta) = & - \frac{1}{R} \sum_{n=1}^{\infty} \frac{P_{2n-1}^1(\cos \theta)}{2n(2n-1) \sin \theta} \times \\ & \left[\left(\frac{1-s}{s} \right)^{2n+1} \int_0^s \frac{ds' s'^{2n-1}}{(1-s')^{2n+1}} \int_0^{\pi/2} d\theta' \sin \theta' P_{2n-1}^1(\cos \theta') \tilde{\sigma}_{\tilde{N}^\phi}(s', \theta') + \right. \\ & \left. \left(\frac{s}{1-s} \right)^{2n-2} \int_s^1 \frac{ds' (1-s')^{2n-2}}{s'^{2n}} \int_0^{\pi/2} d\theta' \sin \theta' P_{2n-1}^1(\cos \theta') \tilde{\sigma}_{\tilde{N}^\phi}(s', \theta') \right], \end{aligned} \quad (\text{A3})$$

$$\begin{aligned} G(s, \theta) = & 1 - \frac{2}{\pi} \sum_{n=1}^{\infty} \frac{\sin[(2n-1)\theta]}{(2n-1) \sin \theta} \times \\ & \left[\left(\frac{1-s}{s} \right)^{2n} \int_0^s \frac{ds' s'^{2n-1}}{(1-s')^{2n+1}} \int_0^{\pi/2} d\theta' \sin[(2n-1)\theta'] \tilde{\sigma}_{\tilde{G}}(s', \theta') \right. \\ & \left. + \left(\frac{s}{1-s} \right)^{2n-2} \int_s^1 \frac{ds' (1-s')^{2n-3}}{s'^{2n-1}} \int_0^{\pi/2} d\theta' \sin[(2n-1)\theta'] \tilde{\sigma}_{\tilde{G}}(s', \theta') \right], \end{aligned} \quad (\text{A4})$$

$$\begin{aligned} \zeta(s, \theta) = & \frac{2}{\pi} \left[\ln r(s) \int_0^s \frac{ds'}{(1-s')^2} \int_0^{\pi/2} d\theta' \tilde{\sigma}_\zeta(s', \theta') \right. \\ & \left. + \int_s^1 \frac{ds'}{(1-s')^2} \ln r(s') \int_0^{\pi/2} d\theta' \tilde{\sigma}_\zeta(s', \theta') \right] \\ & - \frac{2}{\pi} \sum_{n=1}^{\infty} \frac{\cos(2n\theta)}{2n} \left[\left(\frac{1-s}{s} \right)^{2n} \int_0^s \frac{ds' s'^{2n}}{(1-s')^{2n+2}} \int_0^{\pi/2} d\theta' \cos(2n\theta') \tilde{\sigma}_\zeta(s', \theta') \right. \\ & \left. + \left(\frac{s}{1-s} \right)^{2n} \int_s^1 \frac{ds' (1-s')^{2n-2}}{s'^{2n}} \int_0^{\pi/2} d\theta' \cos(2n\theta') \tilde{\sigma}_\zeta(s', \theta') \right], \end{aligned} \quad (\text{A5})$$

where

$$\tilde{\sigma}_\nu(s, \theta) = r^2 \sigma_\nu(s, \theta), \quad (\text{A6})$$

$$\tilde{\sigma}_{\tilde{N}^\phi}(s, \theta) = r^2 \sigma_{\tilde{N}^\phi}(s, \theta), \quad (\text{A7})$$

$$\tilde{\sigma}_{\tilde{G}}(s, \mu) = r \sigma_{\tilde{G}}(s, \theta), \quad (\text{A8})$$

in which the quantities on the right hand side are given by equations (12-14). The symbols $P_n(x)$

and $P_n^m(x)$ denote the Legendre polynomial and the associated Legendre function, respectively. The source $\tilde{\sigma}_\zeta$ requires special consideration. The Green’s function of the 2D Laplacian has a $\ln r$ term, as is apparent from equation (A5). This term must vanish as $r \rightarrow \infty$ in order to have vanishing boundary conditions at infinity. This is not a problem for equation (5) for \tilde{G} , since the $\sin \theta$ factor in the source $\sigma_{\tilde{G}}$ [see equation (14)] guarantees that the $\ln r$ term vanishes everywhere. However, there is no such factor in the source σ_ζ [see equation (6)]. A genuine solution to equation (6) satisfying the boundary condition $\zeta|_{r \rightarrow \infty} \rightarrow 0$ will have a $\ln r$ term that vanishes as $r \rightarrow \infty$; but in the intermediate steps of an iterative procedure to solve the nonlinear equations there is no guarantee that this will be so, leading to a potential instability.

Bonazzola et al. (1993) have a resolution of this difficulty which we adopt here. In order for the $\ln r$ term to vanish as $r \rightarrow \infty$ it is necessary that

$$\int_0^\infty \int_0^{2\pi} \sigma_\zeta(r, \theta) r \, dr \, d\theta = 0. \quad (\text{A9})$$

This condition is called the “virial theorem” by Bonazzola et al. (1993). In terms of the variable s it can be written as

$$\int_0^1 \frac{ds \, s}{(1-s)^3} \sigma_{\zeta,0}(s) = 0, \quad (\text{A10})$$

where

$$\sigma_{\zeta,0}(s) = \int_0^{2\pi} d\theta \, \sigma_\zeta(s, \theta). \quad (\text{A11})$$

The trick is to divide the source σ_ζ into two pieces. One piece, σ_ζ^m , contains the “matter terms” (those involving components of the stress-energy tensor); the other piece, σ_ζ^f , contains the “field terms,” those involving only the metric variables. The virial theorem can then be written

$$\int_0^1 \frac{ds \, s}{(1-s)^3} \sigma_{\zeta,0}^m(s) = - \int_0^1 \frac{ds \, s}{(1-s)^3} \sigma_{\zeta,0}^f(s). \quad (\text{A12})$$

This equation will be satisfied for the actual solution to the Einstein equations, but will not be satisfied in the intermediate steps of the iteration procedure. To avoid the potential logarithmic divergence associated with the failure to satisfy equation (A12), the source σ_ζ is replaced by $\sigma^m + \lambda \sigma^f$, where

$$\lambda = - \left[\int_0^1 \frac{ds \, s}{(1-s)^3} \sigma_{\zeta,0}^m(s) \right] / \left[\int_0^1 \frac{ds \, s}{(1-s)^3} \sigma_{\zeta,0}^f(s) \right]. \quad (\text{A13})$$

In this way equation (A10) is satisfied at each step of the iteration—avoiding the potential logarithmic singularity—but with $\lambda \neq 1$ in the intermediate steps. At the end of the iteration process λ must approach 1 for the computed metric functions to represent a valid solution to the Einstein equations. Finally, $\tilde{\sigma}_\zeta$ in equation (A5) is given by $\tilde{\sigma}_\zeta = R r (\sigma_\zeta^m + \lambda \sigma_\zeta^f)$.

It is convenient to know ahead of time the location of the equatorial surface on the grid. To achieve this we employ a scheme like that Bonazzola et al. (1993) use to divide their computational domain into “inner” and “outer” grids. Specifically, we specify that the equatorial surface be

located at the radial position $s = 0.5$. From equation (A1), this makes the equatorial radius equal to R . Since R is some chosen constant, this involves a nonstandard system of units. Operationally, the value of Newton’s constant G_N is adjusted at each iteration in such a way that $s = 0.5$ does indeed correspond to the equatorial radius of the neutron star, identified by $h = 0$, where h is defined by equation (37). The physical value of the equatorial radius scales as $\sqrt{G_N}$; other physical quantities also involve various powers of G_N .

The scheme is implemented as follows. As with σ_ζ described above, the source term σ_ν is divided into two parts, with the “matter part” σ_ν^m containing source terms deriving from the stress-energy tensor, and the “field part” σ_ν^f containing terms involving derivatives of the metric variables. The Poisson equation for ν is solved in two parts: $\Delta_3\nu^m = \hat{\sigma}_\nu^m$, where $\hat{\sigma}_\nu^m = \sigma_\nu^m/G_N$; and $\Delta_3\nu^f = \sigma_\nu^f$. The full value of ν is then $\nu = G_N\nu^m + \nu^f$. The demand that h vanish at $s = s_* = 0.5$ in the equatorial plane, together with equation (39), yields the appropriate value of Newton’s constant at each iteration:

$$G_N = \frac{(h + \nu^f - \ln \Gamma + M)|_{s=s_{\max}} - (\nu^f - \ln \Gamma + M)|_{s=s_*}}{\nu^m|_{s=s_*} - \nu^m|_{s=s_{\max}}}. \quad (\text{A14})$$

In this expression, $h|_{s=s_{\max}}$ is an input parameter that, via equation (37) and the equation of state, specifies the maximum density in the equatorial plane. This is not necessarily the central density; its location s_{\max} must be determined at each iteration. Specifying the maximum density while allowing its location to “float” allows for the possibility of toroidal configurations, a possibility excluded by the method of Bonazzola et al. (1993) and Bocquet et al. (1995).

In order to test the ability of our code to solve the Einstein equations for axisymmetric configurations, we have studied uniformly rotating configurations with a polytropic EOS and two tabulated “realistic” EOS from the literature. Physical characteristics of the maximum mass configurations for both nonrotating and rotating stars are listed in Table 3, and compared with the results of two other groups. While there is excellent agreement across the board, the agreement is particularly good in the polytropic case. Slightly larger differences in the case of the tabulated EOS are well-attested in the literature, resulting from different methods of interpolation, matching between different density regimes, etc. We tried two methods of determining the “heat function” h from the tabulated EOS: 1) direct integration of equation (37), and 2) use of an analytic formula derived from equation (37) with the first law of thermodynamics. Bocquet et al. (1995) used the analytic formula, and when employing this method we obtained closer agreement with the results of those authors. However, we achieved smaller values of $|1 - \lambda|$ (indicating better solutions) when constructing h by direct integration. This was apparently the method employed by Cook, Shapiro, & Teukolsky (1994b), as our results with this method agree more closely with theirs. Our calculations underlying the entries in Table 3—and, indeed, our calculations with tabulated EOS reported throughout this work—employed the construction of h by direct integration.

In our experience the calculations of rotating configurations with tabulated EOS had a tendency towards numerical instability for large angular velocities, manifested as growing oscillations in various quantities (as opposed to the monotonic runaway occurring past the Keplerian limit). We

found that this instability could be controlled by updating the metric variable N^ϕ only once every n iterations, where we took n as high as 15 when approaching the Keplerian limit. This procedure was not necessary with the polytropic EOS we used.

We also tested our code’s ability to reliably compute static neutron star configurations with large magnetic fields. As reported in the main text, our results for the maximum mass of neutron stars with constant current function f_0 are larger than those reported by Bocquet et al. (1995). Hence comparison of these maximum mass configurations does not really constitute a verification of our code. However, Bocquet et al. (1995) also presented results for the maximum mass at a certain fixed low values of magnetic moment, and comparison of these results provides a benchmark against which our code can be checked. In addition, we can compute configurations close to those reported by Bocquet et al. (1995) as the maximum mass, and make a comparison—even though these are not our maximum mass configurations.

The results of these calculations are presented in Table 4. For each EOS, three sets of calculations are presented. The first set contains results of stars without magnetic fields—the same data appearing in Table 3—as a baseline. The second set shows results for the maximum mass at a given fixed (relatively low) value of magnetic moment. The third set for each EOS has two entries of our calculations. These two configurations represent the boundaries of the range of configurations, at fixed magnetic moment, whose baryon mass rounds to the value reported by Bocquet et al. (1995) as the maximum baryon mass among all configurations with constant current function. The results are satisfactorily concordant. For a visual comparison, our Figure 1 can be checked against Figures 5 and 6 of Bocquet et al. (1995).

We have cited three classes of tests which validate our code. First, the quantity $|1 - \lambda|$ is close to zero as required of valid solutions. Second, our results for quantities characterizing the maximum mass configuration among uniformly rotating stars agree well with those of two previous groups. Third, quantities characterizing certain configurations with magnetic fields reported by Bocquet et al. (1995) show good agreement.

REFERENCES

- Akmal, A., Pandharipande, V. R., & Ravenhall, D. G. 1998, *Phys. Rev. C* 58, 1804
- Alfvén, H. 1950, *Cosmical Electrodynamics* (Oxford: Clarendon)
- Bardeen, J. M. & Wagoner, R. V. 1971, *ApJ*, 167, 359
- Baumgarte, T. W., Shapiro, S. L., & Masaru, S. 2000, *ApJ*, 528, L29
- Baym, G., Bethe, H. A., & Pethick, C. 1971, *Nucl. Phys. A*, 175, 225
- Baym, G., Pethick, C., & Sutherland, P. 1971, *ApJ*, 170, 299

- Bethe, H. A. & Johnson, M. B. 1974, *Nucl. Phys. A*, 230, 1
- Bocquet, M., Bonazzola, S., Gourgoulhon, E., & Novak, J. 1995, *A&A*, 301, 757 (BBG)
- Böhm-Vitense, E. 1989, *Introduction to Stellar Astrophysics*, Vol. 1 (Cambridge: Cambridge UP), Ch. 14
- Bonazzola, S., Gourgoulhon, E., & Marck, J. A. 1998, *Phys. Rev. D*, 58, 104020
- Bonazzola, S., Gourgoulhon, E., Salgado, M., & Marck, J. A. 1993, *A&A*, 278, 421
- Bonazzola, S. & Maschio, G. 1971, in *The Crab Nebula*, ed. R. D. Davies & F. G. Smith (Dordrecht: Reidel), 346
- Bonazzola, S. & Schneider, J. 1974, *ApJ*, 191, 273
- Broderick, A., Prakash, M., & Lattimer, J. M. 2000, *ApJ*, 537, 351
- Cardall, C. Y., Broderick, A., Prakash, M., & Lattimer, J. M. 2000, to be published
- Carroll, B. W. & Ostlie, D. A. 1996, *An Introduction to Modern Astrophysics* (Reading: Addison-Wesley), §15.6
- Carter, B. 1973, in *Black Holes*, ed. C. DeWitt & B. S. DeWitt (New York: Gordon and Breach), 125
- Chakrabarty, S. 1996, *Phys. Rev. D*, 54, 1306
- Chakrabarty, S., Bandyopadhyay, D., & Pal, S. 1997, *Phys. Rev. Lett.*, 78, 2898
- Chandrasekhar, S. & Fermi, E. 1953, *ApJ*, 118, 116
- Chatterjee, P., Hernquist, L., & Narayan, R. 2000, *ApJ*, 534, 373
- Cline, T., Frederiks, D. D., Golenetskii, S., Hurley, K., Kouveliotou, C., Mazets, E., van Paradijs, J. 2000, *ApJ*, 531, 407
- Cook, G. B., Shapiro, S. L., & Teukolsky, S. A. 1992, *ApJ*, 398, 203
- Cook, G. B., Shapiro, S. L., & Teukolsky, S. A. 1994a, *ApJ*, 422, 227
- Cook, G. B., Shapiro, S. L., & Teukolsky, S. A. 1994b, *ApJ*, 424, 823
- Corbel, S., Chapuis, C., Dame, T. M., & Durouchoux, P. 1999, *ApJ*, 526, L29
- Cowling, T. G. 1934, *MNRAS*, 94, 39
- Duncan, R. C. & Thompson, C. 1992, *ApJ*, 392, L9
- Friedman, J. L., Ipser, J. R., & Parker, L., *ApJ*, 304, 115

- Friedman, J. L., Ipser, J. R., & Sorkin, R. D. 1988, ApJ, 325, 722
- Gaensler, B. M., Gotthelf, E. V. & Vasisht, G. 1999, ApJ, 526, L37
- Goldreich, P., & Reisenegger, A. 1992, ApJ, 395, 250
- Gotthelf, E. V. & Vasisht, G. 1998, New Astr. 3, 293
- Gotthelf, E. V., Vasisht, G. & Dotani, T. 1999, ApJ 522, L49
- Haberl, F., Motch, C., Buckley, D. A. H., Zickraf, F.-J., & Pietsch, W. 1997, A&A, 326, 662
- Haberl, F., Pietsch, W. & Motch, C. 2000, A&A 351, L53
- Harding, A. K., Contopoulos, I. & Kazanas, D. 1999, ApJ, 525, L125
- Heyl, J. S. & Hernquist, L. 1998, MNRAS, 297, L69
- Heyl, J. S. & Kulkarni, S. R. 1998, ApJ, 506, L61
- Hurley, K.: 2000, in R. M. Kippen, R. S. Mallozzi, & G. J. Fishman (eds.), *Gamma-Ray Bursts*, in press; astro-ph/9912061
- Hurley, K., Strohmayer, T., Li, P., Kouveliotou, C., Woods, P., van Paradijs, J., Murakami, T., Hartmann, D., Smith, I., Ando, M., Yoshida, A., Sugizaki, M. 2000, ApJ, 528, L21
- Imamura, J., Durisen, R. H., & Friedman, J. L. 1985, ApJ, 294, 474
- Ipser, R., & Lindblom, L. 1989, Phys. Rev. Lett. 62, 2777
- Kaspi, V. M., Lackey, J. R. & Chakrabarty, D. 2000, ApJ, 537, L 31
- Komatsu, H., Eriguchi, Y., & Hachisu, I. 1989, MNRAS, 237, 355
- Kouveliotou, C., Bishman, G. J., B Meegan, C. A., Paciesas, W. S., B van Paradijs, J.; Norris, J. P., B Preece, R. D., Briggs, M. S., B Horack, J. M., Pendleton, G. H., B Green, D. A. 1994, Nature, 368, 125
- Kouveliotou, C. Dieter, S., Strohmayer, T., van Paradijs, J., Fishman, G. J., Meegan, C. A., Hurley, K. 1998, Nature, 393, 235
- Kouveliotou, C. Strohmayer, T., Hurley, K., van Paradijs, J., Finger, M. H., Dieters, S., Woods, P., Thompson, C., Duncan, R. C. 1999, ApJ, 510, L115
- Lindblom, L., & Detweiler, S. L. 1977, ApJ, 211, 565
- Malone, R. C., Johnson, M. B., & Bethe, H. A. 1975, ApJ, 199, 741
- Marsden, D., Lingenfelter, R. E., Rothschild, R. E., & Higdon, J. C. 1999a, preprint (astro-ph/9912207)

- Marsden, D., Rothschild, R. E., & Lingenfelter, R. E. 1999b, *ApJ*, 520, L107
- Oosterbroek, T., Parmar, A. N., Mereghetti, S. & Israel, G. L. 1998, *A&A* 334, 925
- Paczyński, B. 1992, *Acta Astron.*, 42, 145
- Pandharipande, V. R. 1971, *Nucl. Phys. A*, 174, 641
- Parmar, A. N., Oosterbroek, T., Favata, F., Pightling, S., Coe, M. J., Mereghetti, S., Israel, G. L. 1998, *A&A* 330, 175
- Paul, B., Kawasaki, M., Dotani, T., & Nagase, F. 2000, *ApJ*, 537, 319
- Prakash, M., Cooke, J. R., & Lattimer, J. M. 1995, *Phys. Rev. D* 52, 661
- Rothschild, R. E., Kulkarni, S. R., & Lingenfelter, R. E. 1994, *Nature*, 368
- Salgado, M., Bonazzola, S., Gourgoulhon, E., & Haensel, P. 1994, *A&A*, 291, 155
- Sawyer, R. F. 1989, *Phys. Rev. D* 39, 3804
- Shapiro, S. L. & Teukolsky, S. A. 1983, *Black Holes, White Dwarfs, and Neutron Stars* (New York: John Wiley & Sons), §10.5
- Shapiro, S. L., Teukolsky, S. A., & Winicour, J. 1995, *Phys. Rev. D*. 52, 6982
- Sorkin, R. D. 1982, *ApJ*, 257, 847
- Spruit, H. C. 1999a, *A&A*, 341, L1
- Spruit, H. C. 1999b, *A&A*, 349, 189
- Sugizaki, M., Nagase, F., Torii, K., Kinugasa, K., Asanuma, T., Matsuzaki, K., Koyama, K., Yamauchi, S. 1997, *Publ. Astron. Soc. Japan.*, 49, L25
- Taylor, J. H., Manchester, R. N., & Lyne, A. G. 1993, *ApJS*, 88, 529
- Thompson, C. & Duncan, R. C. 1995, *MNRAS*, 275, 255
- Thompson, C. & Duncan, R. C. 1996, *ApJ*, 473, 322
- Torii, K., Kinugasa, K., Katayama, K., Tsunemi, H., Yamauchi, S. 1998, *ApJ* 503, 843
- Usov, V. V. 1992, *Nature*, 357, 472
- Vasisht, G. & Gotthelf, E. V. 1997, *ApJ*, 486, L129
- Vasisht, G., Kulkarni, S. R., Anderson, S. B., & Hamilton, T. T. 1997, *ApJ*, 476, L43
- White, N. E. Angelini, L., Ebisawa, K., Tanaka, Y., Ghosh, P. 1996, *ApJ*, 463, L83

Woods, P. M., Kouveliotou, C., van Paradijs, J., Finger, M. H., Thompson, C. 1999, ApJ, 518, L103

Woods, P. M., Kouveliotou, C., van Paradijs, J., Finger, M. H., Thompson, C., Duncan, R. C., Hurley, K., Strohmayer, T., Swank, J., Murakami, T. 1999, ApJ, 524, L55

Yuan, Y. F., & Zhang, J. L. 1999, ApJ, 525, 920

Zimanyi, J. & Moszkowski, S. A. 1990, Phys. Rev. C 42, 416

Table 1. Properties of soft γ -ray repeaters (SGRs) and anomalous X-ray pulsars (AXPs) from the recent literature*. Question marks indicate uncertain or unconfirmed values.

SGR	P (s)	\dot{P} ^a (10^{-11} s/s)	B ^b (10^{14} G)	D ^c (kpc)	L_X ^d (10^{34} erg/s)	Supernova Remnant (SNR)	Comments
1806-20	7.48	2	8	14	20	G10.0-0.3	
1900+14	5.16	6.1	8	5	3	G42.8+0.6?	27-Aug-98 giant flare; radio point source
0525-66	8		4.5	55	~ 300	N49 in LMC	05-Mar-79 giant flare
1627-41	6.4?			11	10	G337.0-0.1	
1801-23				10?			very recent; only two bursts
AXP							
4U 0412+61	8.69	0.23	2.8	4	112	none	$L_{BB} \sim 40\% L_X$. \dot{P} constant.
1E 1048.1-5937	6.45	1.67/3.29/1.67	6.5	10	8	none	$L_{BB} \sim 55\% L_X$. Three epochs of different, but constant, \dot{P} .
1RXS J170849-4009	11.00	1.9	9.2	10	140	none	$L_{BB} \sim 55\% L_X$. Regular spindown, except for a glitch.
1E 1841-045	11.77	4.1	14	7	35	Kes 73	
AX J1845.0-0258	6.97			15	30	G29.6+0.1	No \dot{P} to date but young SNR, hence large \dot{P} .
1E 2259+586	6.97	0.06	1.3	4	3.3	CTB 109	$L_{BB} \sim 40\% L_X$. Bumpy spin-down.
Magnetar candidates							
RX J0720.4-3125	8.39			0.1	0.0026	none	Blackbody (BB) spectrum, proposed old magnetar
RX J0420.0-5022	22.7?			4	0.4	none	Needs confirmation. Candidate because of large P .

*The entries in this table are extracted from Cline, et al. (2000); Corbel, Chapuis, Dame, & Durouchoux (1999); Gaensler, Gotthelf, & Vasisht (1999); Gotthelf & Vasisht (1998); Gotthelf, Vasisht, & Dotani (1999); Haberl, Motch, Buckley, Zickraf, & Pietsch (1997); Haberl, Pietsch, & Motch (2000); Hurley (2000); Hurley et al. (2000); Heyl & Hernquist (1998); Kaspi, Lackey, & Chakrabarty (2000); Kouveliotou et al. (1998, 1999); Oosterbroek, Parmar, Mereghetti, & Israel (1998); Parmar et al. (1998); Paul, Kawasaki, Dotani, & Nagase (2000); Rothschild, Kulkarni, & Lingenfelter (1994); Sugizaki, et al. (1997); Torii et al. (1998); Vasisht & Gotthelf (1997); Vasisht, Kulkarni, Anderson, & Hamilton (1997); White et al. (1996); Woods et al. (1999a,b)

^aIn most cases there is not enough sampling of \dot{P} to allow strong claims of constancy in time, and in many cases there is evidence of significant variations.

^b B is obtained by standard magnetodipolar radiation braking, only good to within an order of magnitude.

^cDistances are poorly determined (with the exception of SGR 0525-66 in the LMC).

^dThe X-ray luminosity L_X scales as D^2 and is estimated from the observed unabsorbed flux using the quoted distance.

Table 2. Maximum mass models at various fixed values of magnetic moment.

EOS	\mathcal{M} (10^{35} Gaussian)	h_{\max}	e_{\max} (1.66×10^{14} g cm $^{-3}$)	B_c (10^{16} G)	B_{pole} (10^{16} G)	M (M_{\odot})	M_B (M_{\odot})	R (km)	$ 1 - \lambda $
Pol2	0.00	0.492	10.5	0.00	0.00	2.00	2.19	13.8	1E-4
	2.00	0.459	9.41	150	36.9	2.12	2.28	13.9	6E-5
	3.00	0.511	11.1	253	122	2.37	2.38	12.8	2E-4
	4.00	0.386	7.28	180	92.9	2.56	2.66	15.2	3E-4
	<i>4.99</i>	<i>0.291</i>	<i>4.94</i>	<i>129</i>	<i>70.6</i>	<i>2.64</i>	<i>2.78</i>	<i>17.6</i>	<i>3E-4</i>
	5.00	0.290	4.92	129	70.4	2.64	2.78	17.6	3E-4
	<i>6.18</i>	<i>0.143</i>	<i>2.07</i>	<i>59.6</i>	<i>34.4</i>	<i>2.31</i>	<i>2.43</i>	<i>22.9</i>	<i>3E-4</i>
BJI	0.00	0.687	18.5	0.00	0.00	1.86	2.14	9.92	5E-4
	1.50	0.568	14.6	236	84.1	1.96	2.17	10.3	4E-5
	2.00	0.706	19.2	419	249	2.12	2.05	9.53	4E-4
	2.50	0.586	15.1	335	216	2.28	2.29	10.7	5E-4
	3.00	0.476	11.9	269	181	2.38	2.47	11.9	6E-4
	<i>3.29</i>	<i>0.408</i>	<i>10.1</i>	<i>232</i>	<i>157</i>	<i>2.40</i>	<i>2.54</i>	<i>12.6</i>	<i>1E-3</i>
	<i>3.70</i>	<i>0.265</i>	<i>6.68</i>	<i>156</i>	<i>104</i>	<i>2.25</i>	<i>2.41</i>	<i>14.4</i>	<i>2E-4</i>
PandN	0.00	0.728	24.9	0.00	0.00	1.66	1.92	8.36	5E-5
	1.00	0.617	20.3	292	87.8	1.72	1.92	8.72	8E-5
	1.50	0.724	24.7	504	303	1.86	1.80	8.18	3E-4
	2.00	0.590	19.3	386	271	2.05	2.06	9.37	4E-4
	<i>2.49</i>	<i>0.422</i>	<i>13.7</i>	<i>281</i>	<i>202</i>	<i>2.13</i>	<i>2.23</i>	<i>10.8</i>	<i>5E-4</i>
	2.50	0.410	13.4	276	197	2.12	2.23	10.8	5E-4
	<i>2.82</i>	<i>0.231</i>	<i>8.31</i>	<i>166</i>	<i>119</i>	<i>1.90</i>	<i>2.03</i>	<i>12.6</i>	<i>2E-4</i>
Akmal	0.00	0.910	16.7	0.00	0.00	2.20	2.67	10.0	2E-4
	1.20	0.792	14.3	228	59.3	2.22	2.62	10.3	7E-5
	2.00	0.648	11.8	338	134	2.31	2.58	10.6	3E-4
	2.80	0.674	12.3	370	244	2.53	2.59	11.0	2E-4
	3.60	0.550	10.3	287	221	2.73	2.84	12.4	3E-4
	<i>3.71</i>	<i>0.514</i>	<i>9.75</i>	<i>271</i>	<i>209</i>	<i>2.73</i>	<i>2.88</i>	<i>12.6</i>	<i>3E-4</i>
	<i>4.10</i>	<i>0.307</i>	<i>6.81</i>	<i>179</i>	<i>132</i>	<i>2.52</i>	<i>2.73</i>	<i>14.3</i>	<i>1E-3</i>
PCL	0.00	0.561	17.3	0.00	0.00	1.72	1.95	10.4	4E-4
	1.70	0.665	22.7	418	218	1.91	1.86	9.14	4E-4
	2.20	0.547	16.6	327	186	2.09	2.12	10.4	6E-4
	2.70	0.445	12.5	259	155	2.21	2.31	11.7	8E-4
	3.20	0.350	9.22	201	124	2.26	2.41	13.1	5E-4
	<i>3.31</i>	<i>0.335</i>	<i>8.75</i>	<i>192</i>	<i>120</i>	<i>2.28</i>	<i>2.43</i>	<i>13.4</i>	<i>4E-4</i>
	<i>3.86</i>	<i>0.202</i>	<i>5.12</i>	<i>116</i>	<i>74.7</i>	<i>2.09</i>	<i>2.24</i>	<i>15.8</i>	<i>1E-4</i>
PCLhyp	0.00	0.504	17.6	0.00	0.00	1.59	1.78	10.3	4E-4
	1.50	0.620	24.3	416	202	1.76	1.73	8.82	5E-4
	2.00	0.488	16.7	308	161	1.93	1.98	10.3	5E-4
	2.50	0.387	12.1	235	130	2.04	2.15	11.8	3E-4
	3.00	0.310	8.97	182	106	2.11	2.25	13.2	8E-6
	<i>3.39</i>	<i>0.263</i>	<i>7.29</i>	<i>152</i>	<i>93.1</i>	<i>2.13</i>	<i>2.28</i>	<i>14.2</i>	<i>2E-4</i>
	<i>3.81</i>	<i>0.186</i>	<i>4.83</i>	<i>107</i>	<i>68.7</i>	<i>2.02</i>	<i>2.16</i>	<i>16.1</i>	<i>5E-4</i>

Note. — The quantity h_{\max} is the maximum value of the log-enthalpy per baryon defined in equation (37), e_{\max} is the maximum energy density, B_c and B_{pole} are the magnetic field strengths at the star’s center and pole, respectively, M is the gravitational mass, M_B is the star’s baryon mass, R is the equatorial radius, and $|1 - \lambda|$ is a function defined in equation (A13) describing convergence. The results are grouped by the equation of state (EOS), each of which is described in the text. Entries in plain type correspond to the sequences of constant magnetic moment \mathcal{M} shown in Figures 7 and 8. For each EOS there are two italicized rows which correspond, respectively, to the configurations of maximum mass and maximum magnetic moment among all configurations with constant current function.

Table 3. Maximum mass models, nonrotating and rotating.

EOS	Authors	h_c	e_c ($1.66 \times 10^{14} \text{ g cm}^{-3}$)	Ω (10^4 s^{-1})	M (M_\odot)	M_B (M_\odot)	R (km)	J/M^2 (G_N/c)	$ 1 - \lambda $
Pol2	CST	...	10.6	0.00	1.99	2.19	13.7	0.00	...
	BBGN	0.491	10.4	0.00	2.00	2.19	13.8	0.00	1E-14
	CPL	0.492	10.5	0.00	2.00	2.19	13.8	0.00	1E-4
	CST	...	8.63	0.629	2.29	2.52	19.7	0.572	...
	BBGN	0.432	8.58	0.629	2.30	2.52	19.6	0.570	6E-6
	CPL	0.432	8.58	0.629	2.30	2.53	19.6	0.570	1E-4
BJI	CST	...	18.5	0.00	1.86	2.16	9.93	0.00	...
	BBGN	0.699	18.6	0.00	1.86	2.13	9.91	0.00	2E-6
	CPL	0.687	18.5	0.00	1.86	2.14	9.92	0.00	5E-4
	CST	...	16.0	1.06	2.17	2.49	13.4	0.629	...
	BBGN	0.628	16.3	1.07	2.15	2.46	13.4	0.626	9E-5
	CPL	0.610	15.9	1.07	2.16	2.47	13.4	0.632	4E-5
PandN	CST	...	24.9	0.00	1.66	1.92	8.37	0.00	...
	BBGN	0.733	24.4	0.00	1.66	1.93	8.55	0.00	2E-4
	CPL	0.728	24.9	0.00	1.66	1.92	8.36	0.00	5E-5
	CST	...	21.4	1.32	1.95	2.24	11.2	0.665	...
	BBGN	0.668	21.7	1.29	1.93	2.23	11.4	0.641	7E-5
	CPL	0.647	21.5	1.33	1.96	2.25	11.1	0.666	1E-5

Note. — J is the total angular momentum. See the caption to Table 2 for an explanation of the other quantities tabulated. The subscript c refers to central values. For each EOS, results from this work (CPL) are compared to those of Cook, Shapiro, & Teukolsky (1994a) and Cook, Shapiro, & Teukolsky (1994b) for the polytropic and tabulated EOSs, respectively (together labelled CST), and to Bocquet et al. (1995) (BBGN).

Table 4. Comparison of static models with various magnetic moments.

EOS	Authors	\mathcal{M} (10^{35} Gaussian)	h_c	e_c (1.66×10^{14} g cm $^{-3}$)	B_c (10^{16} G)	B_{pole} (10^{16} G)	M (M_\odot)	M_B (M_\odot)	R (km)	$ 1 - \lambda $
Pol2	CST	0.00	...	10.6	0.00	0.00	1.99	2.19	13.7	...
	BBGN	0.00	0.491	10.4	0.00	0.00	2.00	2.19	13.8	1E-14
	CPL	0.00	0.492	10.5	0.00	0.00	2.00	2.19	13.8	1E-4
BBGN	BBGN	0.800	0.483	10.2	59.8	9.8	2.01	2.21	13.8	1E-6
	CPL	0.800	0.484	10.2	60.4	10.0	2.02	2.21	13.8	2E-4
BBGN	BBGN	4.49	0.225	3.55	142	72.3	2.57	2.71	16.8	1E-3
	CPL	4.49	0.224	3.53	140	70.7	2.56	2.71	16.8	2E-4
	CPL	4.49	0.224	3.53	142	72.6	2.57	2.71	16.8	3E-4
BJI	CST	0.00	...	18.5	0.00	0.00	1.86	2.16	9.93	...
	BBGN	0.00	0.699	18.6	0.00	0.00	1.86	2.13	9.91	2E-6
	CPL	0.00	0.687	18.5	0.00	0.00	1.86	2.14	9.92	5E-4
BBGN	BBGN	0.30	0.692	18.4	61.5	11.0	1.86	2.13	9.94	2E-6
	CPL	0.30	0.680	18.2	60.9	11.1	1.86	2.14	9.95	2E-4
BBGN	BBGN	2.63	0.300	7.47	233	121	2.18	2.34	12.0	1E-4
	CPL	2.63	0.287	7.16	215	110	2.15	2.34	12.3	2E-4
	CPL	2.63	0.292	7.27	222	115	2.17	2.34	12.2	2E-4
PandN	CST	0.00	...	24.9	0.00	0.00	1.66	1.92	8.37	...
	BBGN	0.00	0.733	24.4	0.00	0.00	1.66	1.93	8.55	1E-4
	CPL	0.00	0.728	24.9	0.00	0.00	1.66	1.92	8.36	5E-5
BBGN	BBGN	0.20	0.727	24.1	64.7	11.9	1.66	1.93	8.57	1E-4
	CPL	0.20	0.722	24.6	66.6	12.9	1.66	1.92	8.38	4E-5
BBGN	BBGN	1.86	0.350	11.2	303	154	1.91	2.06	10.0	3E-4
	CPL	1.86	0.328	11.0	292	153	1.90	2.06	10.0	3E-4
	CPL	1.86	0.336	11.2	361	209	1.96	2.06	9.47	3E-4

Note. — See the notes to Tables 2 and 3 for explanations of symbols and abbreviations.

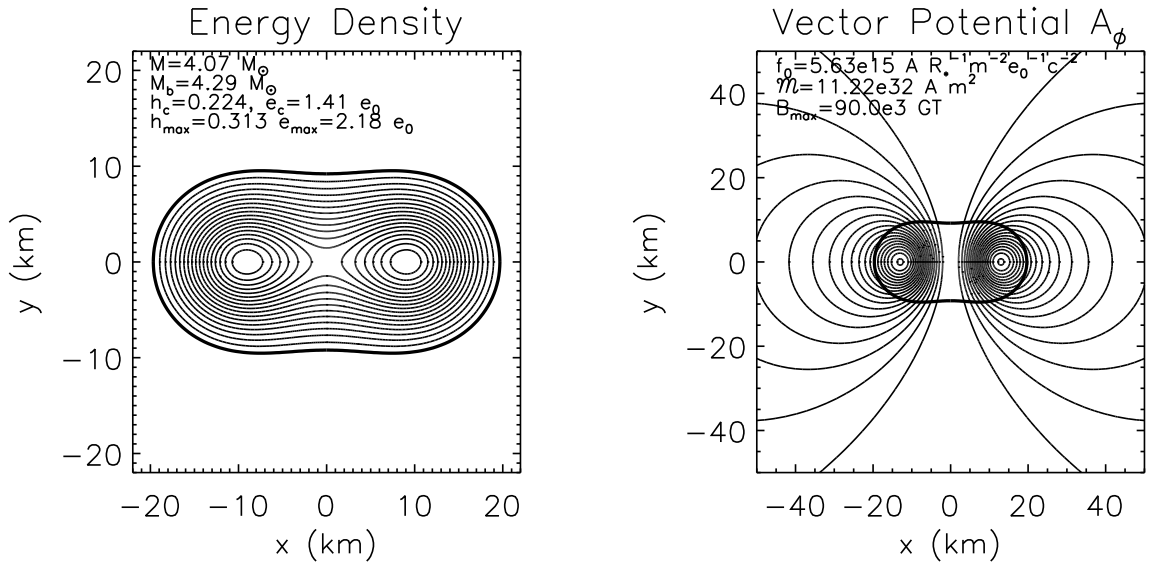


Fig. 1.— Contour plots of the energy density and the electromagnetic vector potential component A_ϕ . Here $x = r \sin \theta$ and $y = r \cos \theta$, where r and θ are coordinates appearing in equation (2); note that in these coordinates not even distances in the equatorial plane constitute proper distances. $e_0 = 1.66 \times 10^{14} \text{ g cm}^{-3}$, and R_* is the equatorial radius. While contours of constant A_ϕ show the structure of the magnetic field, their spacing as pictured here does not accurately indicate magnetic field strength; the maximum magnetic field is actually at the center of the star. To allow a direct comparison, with Figures 5 and 6 of Bocquet et al. (1995), we assumed their value of the polytropic constant. Table 4 contains physical quantities rescaled to reflect a more realistic value of this constant).

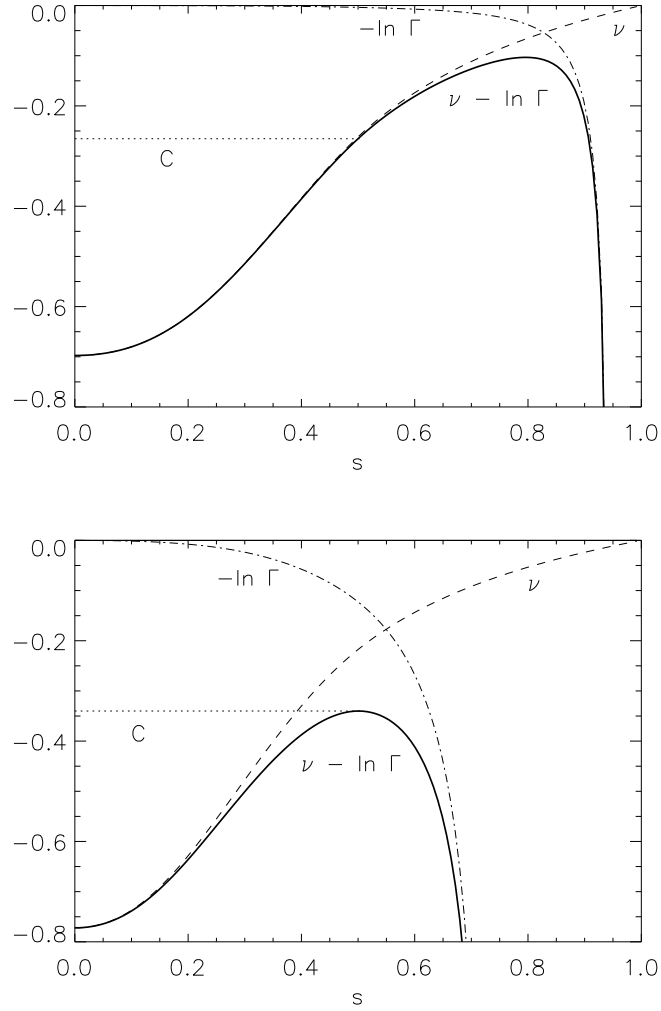


Fig. 2.— Various quantities associated with the Bernoulli equation (42) in the equatorial plane of a uniformly rotating star, as a function of the compactified radial coordinate $s = r/(R_* + r)$, where R_* is the equatorial radius. The upper panel shows a configuration with modest rotation, and the lower panel shows a configuration at the Keplerian limit. See the text for discussion.

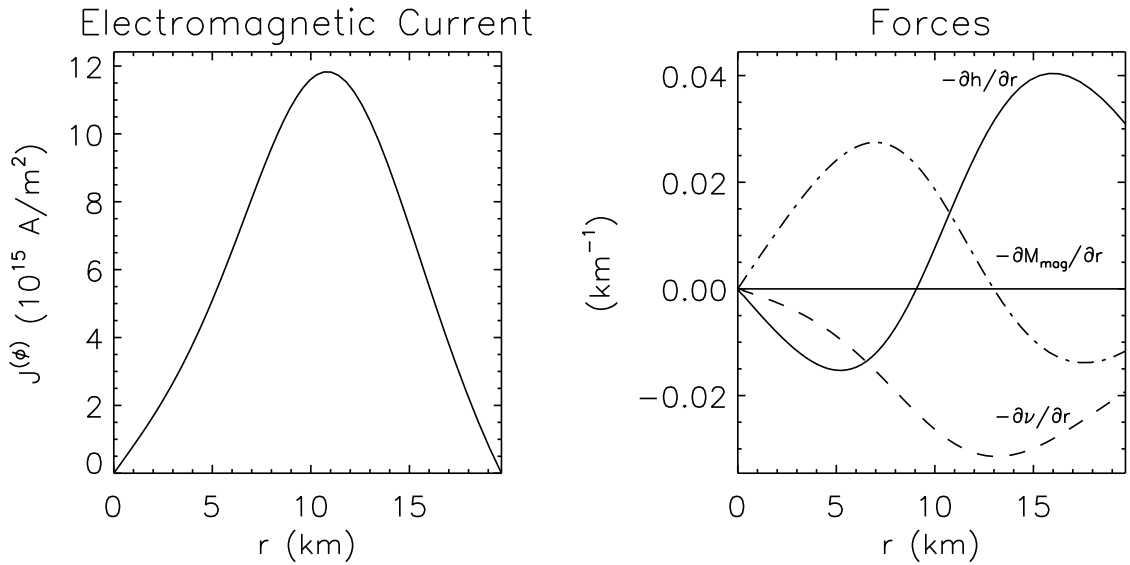


Fig. 3.— The electromagnetic current and various “forces” in the equatorial plane for the configuration pictured in Figure 1. The “forces” are derivatives of the terms in the Bernoulli equation (43); here M is the magnetic potential. The right boundaries correspond to the equatorial radius R_* . Note that the pressure force ($-\partial h / \partial r$) points inward at lower radii; this is a consequence of the maximum density being pushed off center (see the left panel of Figure 1) due to the strong outward Lorentz force ($-\partial M / \partial r$). The Lorentz force also reverses sign, due to a reversal of magnetic field direction in the equatorial plane (see the right panel of Figure 1). At R_* , the Lorentz force works together with gravity to help confine the star, in contrast with the centrifugal force in the case of rapid rotation.

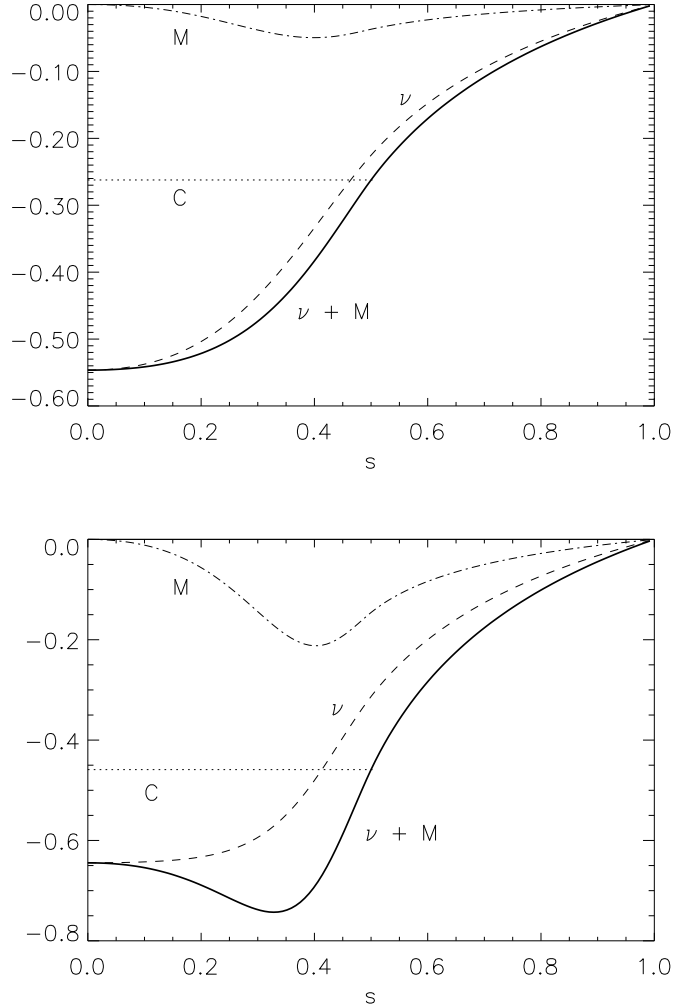


Fig. 4.— Similar to Figure 2, but for the Bernoulli equation (43) of a nonrotating star in a poloidal magnetic field. M is the magnetic potential. The upper panel shows a configuration in which the magnetic field is strong enough to modestly deform the star, while the lower panel displays the configuration with the largest current function for which convergence was achieved (for the same maximum density as the configuration in the upper panel). When compared with Figure 2, the absence of mass shedding is evident.

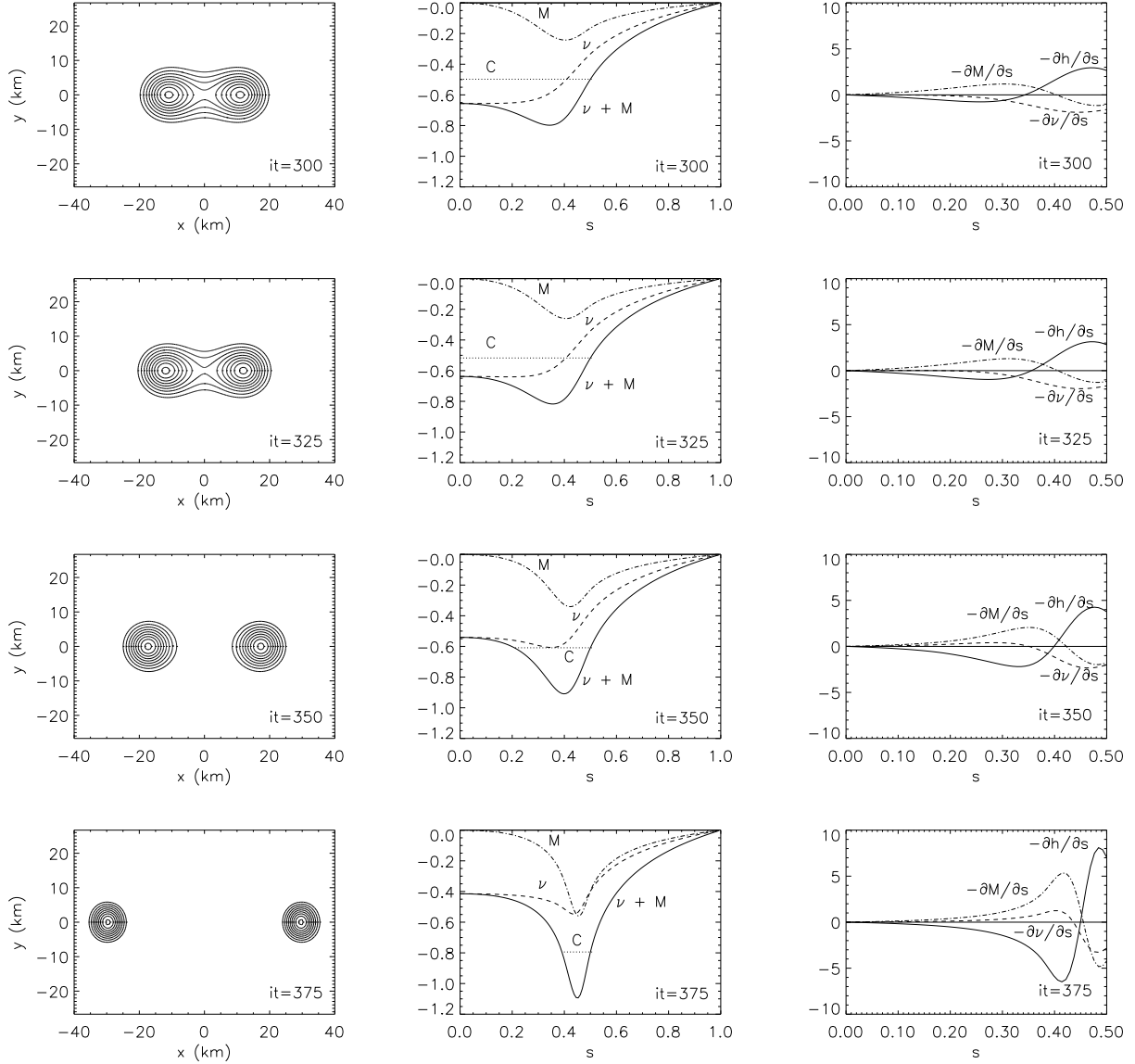


Fig. 5.— Late stages of iteration of a non-converging configuration (as a solution of the Einstein and Maxwell equations). Left panels: Density contour plots show a transition to a toroidal topology as the iterations proceed. Center panels: “Potential” plots similar to Figure 2; note the increasingly narrow well into which the matter is compressed. Right panels: “Force” plots similar to Figure 4; the tendency of the gravitational force to join the magnetic force in pushing matter away from the origin becomes more and more pronounced.

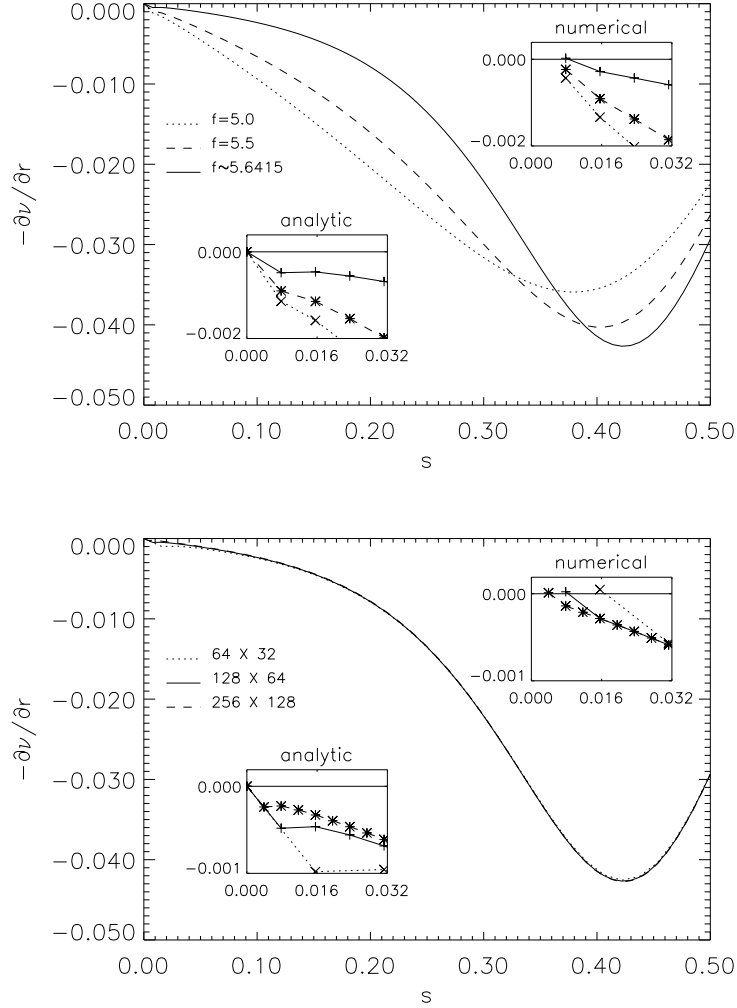


Fig. 6.— The gravitational force in the equatorial plane. Upper panel: The gravitational force for increasing values of f_0 , at a fixed value of maximum stellar density. The indicated values of f_0 are given in units of $10^{15}(R_* e_0 c^2)^{-1} \text{ A m}^{-2}$, where R_* is the coordinate radius of the equatorial surface. The insets show the force near the origin, computed both “analytically” and numerically, as described in the text. Lower panel: The gravitational force for the maximum value of f_0 for which convergence was achieved (for a particular value of maximum density), for configurations computed with three different resolutions in r and θ .

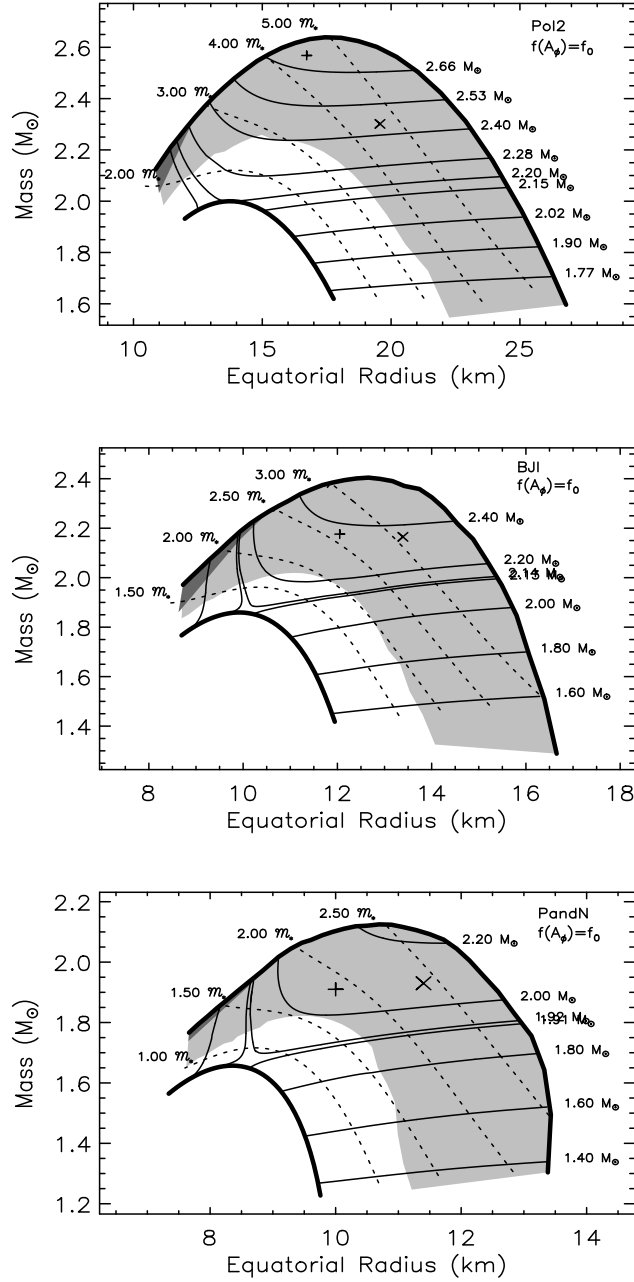


Fig. 7.— Mass-equatorial radius plots showing converged solutions attainable with a constant current function, for EOSs used by Bocquet et al. (1995). The lower heavy line represents spherical, non-magnetized, configurations, and the upper heavy line represents the boundary beyond which solutions appear not to exist (see §3). Lighter solid lines are sequences of constant baryon mass (in M_{\odot}), while dotted lines are sequences of constant \mathcal{M} (in units of $\mathcal{M}_* = 10^{35}$ Gaussian). Lighter shaded regions indicate configurations in which the maximum density is not at the center; the darker shaded regions indicate gravitationally unbound configurations. “X”s denote the maximum mass configuration attainable by uniform rotation, and crosses indicate the maximum masses for non-rotating, magnetized configurations reported by Bocquet et al. (1995).

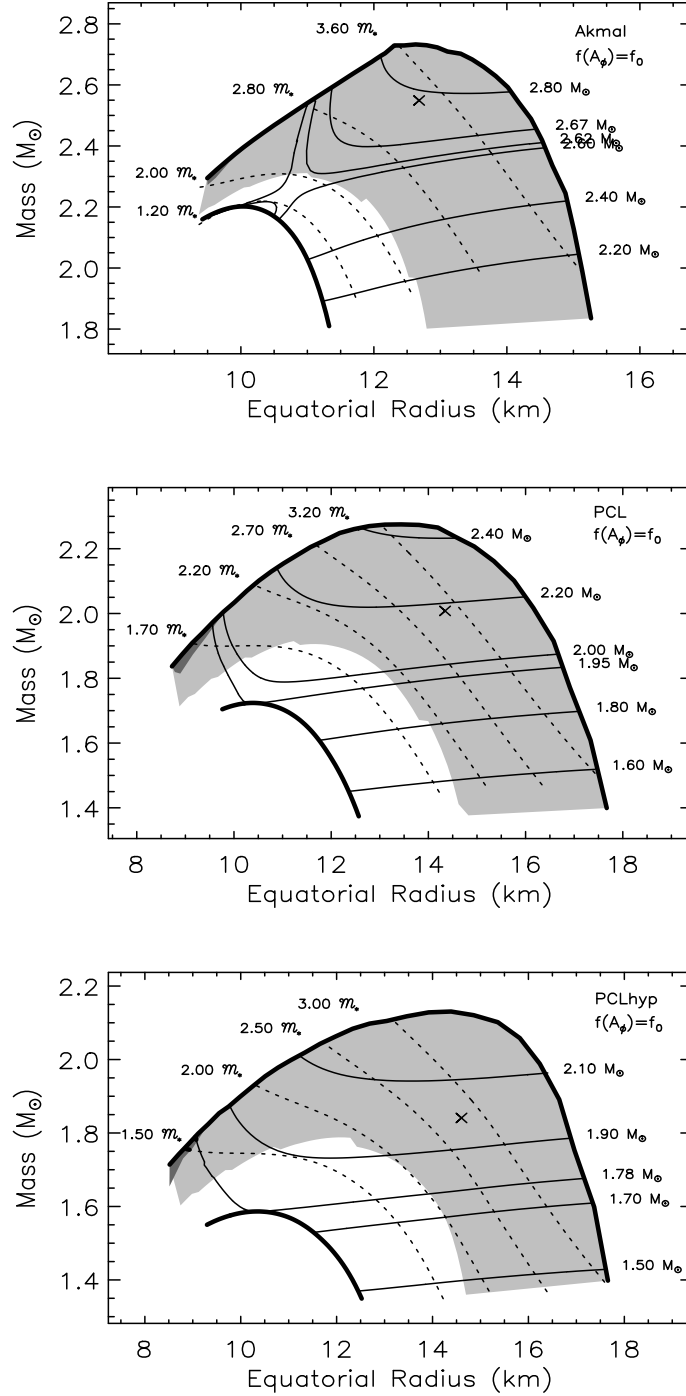


Fig. 8.— Similar to Figure 7, but for three more recent EOSs discussed in the text.